Complete classification of qualitatively different perturbations of the hydrogen atom in weak near-orthogonal electric and magnetic fields

2009 J. Phys. A: Math. Theor. 42 055209

(http://iopscience.iop.org/1751-8121/42/5/055209)

IOP PUBLISHING JOURNAL OF PHYSICS A: MATHEMATICAL AND THEORETICAL

J. Phys. A: Math. Theor. **42** (2009) 055209 (29pp) doi:10.1088/1751-8113/42/5/055209

Complete classification of qualitatively different perturbations of the hydrogen atom in weak near-orthogonal electric and magnetic fields

K Efstathiou[1], **O V Lukina**[1] **and D A Sadovskií**[2]

[1] Department of Mathematics, University of Groningen, Groningen 9700 AK, The Netherlands
[2] Département de physique, Université du Littoral, 59140 Dunkerque, France

E-mail: K.Efstathiou@rug.nl, O.Lukina@math.rug.nl and sadovski@univ-littoral.fr

Received 4 August 2008, in final form 20 November 2008
Published 6 January 2009
Online at stacks.iop.org/JPhysA/42/055209

Abstract

We consider perturbations of the hydrogen atom by sufficiently small homogeneous static electric and magnetic fields in near-orthogonal configurations. Normalization of the Keplerian symmetry reveals that in the parameter space such systems belong in a 'zone' of systems close to the 1:1 resonance, the latter corresponding to the exactly orthogonal configuration. Integrable approximations obtained from second normalization of systems in the 1:1 zone are classified into several different qualitative types, many of which possess nontrivial monodromy. We compute monodromy of the complete three-dimensional energy–momentum map, compare the joint quantum spectrum to classical bifurcation diagrams, and show the effect of second normalization to the joint spectrum.

PACS numbers: 32.60.+i, 02.30.Ik, 02.40.Yy, 03.65.Sq, 03.65.Vf, 45.05.+x

1. Introduction

The general problem of describing different perturbations of the hydrogen atom in the electric and magnetic field was posed by Pauli [1] who worked at the level of the first-order perturbation theory. It was Solov'ev [2] and Herrick [3] who, on the example of the quadratic Zeeman effect, demonstrated the necessity of the second-order perturbation theory for the qualitative understanding of these systems.

A number of studies for specific field configurations followed and a significant step forwards was made in [4] where all orthogonal field perturbations were shown to be of three basic generic types. Namely, systems near the Zeeman and Stark limits similar to those studied in [2, 3], and systems with monodromy. There has been a significant number of studies of this problem from different points of view [5–10]. Here we mention only the most directly related work. A few more distant references are [11–17]. A thorough review of all works

on other aspects of this problem (ionization, chaotic regime, purely quantum computations of low-lying states, etc) is beyond the scope of our work.

The significance of [4] goes beyond the strictly orthogonal case: this work has essentially shown the way to classify *all* perturbations of the H atom by (sufficiently weak, homogeneous and static) electric and magnetic fields of arbitrary mutual orientation, and thus to complete the study initiated by Pauli in 1926 [1]. In the spirit of [4], we construct integrable approximations to these systems using a second-order perturbation theory (and going to higher orders if necessary). Within such an approximation, the phase space is foliated into fibres which are common level sets of the integrals of motion and typically—in three degree of freedom (DOF) systems—three-dimensional tori. The topological properties of this (in general singular) fibration, and in particular monodromy, give the qualitative characteristics of the original perturbed nonintegrable system [18, 19].

Monodromy is a global topological property of integrable [20] and near-integrable [18, 19] Hamiltonian systems. It signifies the absence of smooth global action variables or equivalently the absence of good global quantum numbers for the quantized system. Monodromy is usually associated in 2DOF systems to the existence of focus–focus singularities [21–23] or deformations of such singularities [24]. In [4] it was shown that in the hydrogen atom in orthogonal fields there is a parameter region in which the system has monodromy. In [25] the appearance of monodromy in the system was related to Hamiltonian Hopf bifurcations.

More recently it was shown in [26–28] that near-orthogonal configurations can be considered as deformations of the strictly orthogonal ones which break the specific $\mathbb{Z}_2$ symmetry of the latter. Such deformed systems can be of different qualitative types and can have monodromy of different kinds. Furthermore, in [26] we provided a general framework to classify all perturbations. In the parameter space of all perturbed systems we conjectured the existence of *resonant* $k_1 : k_2$ *zones* within which the system can be approximated using a detuned resonance characterized by two positive integers k_1 and k_2. Note that these resonances and respective quantum systems were studied independently in [29]; the zone concept and the corresponding approach in [26] are new.

The near-orthogonal field configurations correspond to the 1:1 zone which was characterized initially in [26, 27]. We give a complete description in this paper. We consider the hydrogen atom in near-orthogonal fields as a deformation of the case of exactly orthogonal fields. Note that a very similar approach has been used previously in [24] to study monodromy in a family of spherical pendula with quadratic potentials which can be considered as deformations of the usual spherical pendulum with linear gravitational potential. Other model Hamiltonian systems with properties similar to those of the perturbed hydrogen atom, notably with the same reduced phase space $\mathbb{S}^2 \times \mathbb{S}^2$ (see section 3), have been analysed before: in [30] and more recently in [31] the authors study monodromy of a system of coupled angular momenta; in [32] the authors obtain similar results for the geodesic flow on four-dimensional ellipsoids.

Uncovering monodromy in many physical systems such as the CO_2 molecule and the hydrogen atom was a major achievement of the past decade. When present, monodromy becomes the organizing centre of the whole joint spectrum of the quantum system. The physical manifestations of this global phenomenon on the properties of the quantum eigenstates are currently actively investigated. Classifying and describing perturbed hydrogen atom systems with different types of monodromy is, in this context, an important development.

1.1. Hamiltonian and its parameterization

In the limit of the infinite proton mass and with spin and relativistic corrections neglected, the hydrogen atom perturbed by electric and magnetic fields becomes a quantum realisation of a

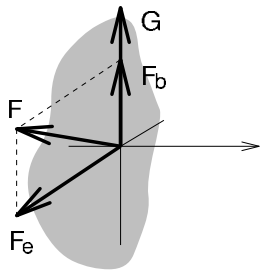

Figure 1. Electric and magnetic fields **F** and **G**.

specific class of perturbations of the Kepler system with Hamiltonian (in atomic units)

$$H_{3D} = \frac{1}{2}\mathbf{P}^2 - \frac{1}{|\mathbf{Q}|} + F_e Q_2 + F_b Q_1 + \frac{1}{2}G(Q_2 P_3 - Q_3 P_2) + \frac{1}{8}G^2(Q_2^2 + Q_3^2) = E, \tag{1}$$

where $\mathbf{Q}$ are Cartesian coordinates in $\mathbb{R}^3$ and $\mathbf{P}$ are their conjugate momenta. The 3-vectors $\mathbf{F} = (F_b, F_e, 0)$ and $\mathbf{G} = (G, 0, 0)$, see figure 1, represent the electric and the magnetic field, respectively. Specifically, $\mathbf{F} = -\mathbf{E}$ and $\mathbf{G} = -\mathbf{B}$ where $\mathbf{E}$ and $\mathbf{B}$ are the electric field and magnetic flux density respectively. We remain at sufficiently large negative physical energy E and consider bounded motion near the origin.

In order to describe the parameter space we introduce the n-scaled field amplitudes[3]

$$g = Gn^2, \qquad (f_e, f_b) = 3(F_e, F_b)n^3. \tag{2}$$

Here n is the value of the Keplerian integral N given by

$$H_0 = \frac{1}{2}\mathbf{P}^2 - \frac{1}{|\mathbf{Q}|} = -\frac{1}{2N^2}. \tag{3}$$

It corresponds to the principal quantum number. Note that N is not an integral of motion for the original Hamiltonian H in (1) but becomes such only after normalization (and truncation), which we call first or Keplerian normalization. Furthermore define

$$s = \left(g^2 + f_b^2 + f_e^2\right)^{1/2} > 0, \qquad a^2 = \frac{g^2}{s^2}, \qquad d = \frac{g f_b}{s^2}, \tag{4a}$$

that satisfy

$$d^2 \leqslant (1 - a^2)a^2. \tag{4b}$$

For each fixed $s > 0$, (4*b*) defines a disc D in the parameter plane with coordinates (d, a^2). Therefore, in coordinates (s, d, a^2) with $s > 0$ the parameter space of all perturbations of the hydrogen atom by electric and magnetic fields is described as a solid cylinder $\mathbb{R}_{>0} \times D$. The parameter s plays the role of a universal parameter which represents the total strength of the perturbation and which should be kept small in order for all normalizations to give a realistic approximation of the dynamics. The use of such universal scalings goes back to [4, 33].

1.2. Normalization and reduction

The normalization of the Hamiltonian in (1) involves the Kustaanheimo–Stiefel regularization of the singularity of the Keplerian potential, and then two successive normalizations that give an integrable Hamiltonian system. The results of this procedure are given in section 3 and the procedure itself is detailed in [34].

[3] Note that in [26] we denoted by (f_e, f_b, g) the energy-scaled fields.

Table 1. Notation.

G, F_e, F_b	Components of the magnetic and electric fields
g, f_e, f_b	n-scaled components of the magnetic and electric fields, see (2).
s, a^2, d	Reparameterization of the system, see (4*a*).
N, n	Keplerian action and its value, see (3).
E	First normalized energy, see (14), (15).
$\mathbb{S}^2 \times \mathbb{S}^2$	The phase space for the first normalized and reduced system defined by E, see section 3.1.
ΔE	First normalized and reduced energy correction function, see (5), (15).
$\Delta E^{(1)}$, $\Delta E^{(2)}$	First- and second-order terms in the first normalized energy correction function ΔE, see (15*b*), (15*c*), and (21).
μ, m	Second integral (momentum) and its value, see (25).
ω_+, ω_-	Frequencies of rotation on $\mathbb{S}^2 \times \mathbb{S}^2$, see (18).
$\Delta\mathcal{E}$	Second normalized and reduced energy correction function, see (29), (30), table 5.
$\Delta\mathcal{E}^{(1)}$, $\Delta\mathcal{E}^{(2)}$	First- and second-order terms in the second normalized energy correction function $\Delta\mathcal{E}$, see (30) and table 5 respectively.
$P_{n,m}$	Second reduced phase space, see section 3.3; N, μ are constant on $P_{n,m}$ with values n, m respectively.
ν, π_1, π_2	Coordinates on $\mathbb{R}^3 \supset P_{n,m}$, see (25) and section 3.3.
$\mathcal{H}$, h	The Hamiltonian function on $P_{n,m}$ and its value. $\mathcal{H}$ is defined as the nontrivial part of $\Delta\mathcal{E}$, i.e., it does not contain the terms of $\Delta\mathcal{E}$ that depend only on n, m and are thus constant on $P_{n,m}$.
$\mathbb{T}^2_{[1]}$, $\mathbb{T}^2_{[2]}$, $\mathbb{T}^2_{\text{bi}}$	Singly pinched torus, doubly pinched torus, bitorus, see figure 7.

The first of these normalizations is made with respect to the Keplerian integral N and it is carried out to second order. Up to the freedom in the choice of generators in the normal form algorithm which does not affect any final physical results, see [34–37], our normal form agrees with that by Solov'ev [2]. Thus we obtain the first normalized energy E which has the form (see also table 1 for the notation)

$$E = -\frac{1}{2n^2} + \frac{1}{2n^2}\Delta E. \tag{5}$$

The quantity ΔE is a Hamiltonian function and is called the *first normalized energy correction function*. Since ΔE commutes with N we can use the integral N to reduce the problem from three degrees of freedom (DOF) to 2-DOF. When doing reduction we do not change ΔE but we just express it in terms of different dynamical variables. These variables are functions in phase space that commute with N. In the case of the hydrogen atom this reduction is well known, see, for example, [4]. Thus after reduction ΔE becomes a Hamiltonian function on the *first reduced phase space* $\mathbb{S}^2 \times \mathbb{S}^2$. The coordinates on $\mathbb{S}^2 \times \mathbb{S}^2$ are the Pauli vectors $(\mathbf{X}, \mathbf{Y})$ that satisfy $\|\mathbf{X}\| = \|\mathbf{Y}\| = n/2$ and their components commute with N, see section 3.1. The value of N is constant n on $\mathbb{S}^2 \times \mathbb{S}^2$. Although the first normalized energy correction and its reduced form are formally different functions, since they are defined on different spaces, we denote them both by ΔE.

A specific characteristic of the system defined by ΔE on $\mathbb{S}^2 \times \mathbb{S}^2$ is that the lowest degree nontrivial term $\Delta E^{(1)}$ (21) in ΔE, generates a linear $\mathbb{S}^1$ action on $\mathbb{S}^2 \times \mathbb{S}^2$ which is the simultaneous rotation of the two spheres about an axis with frequencies ω_- and ω_+ that depend on the fields[4]. In the case of strictly orthogonal fields $\omega_- = \omega_+$, thus we have an 1:1

[4] In the case of only magnetic field, this symmetry is identified with the axial symmetry of the problem and the respective generator is the projection of the angular momentum along the symmetry axis.

resonance. We denote the generator of this resonant 1:1 $\mathbb{S}^1$ symmetry by μ. In general, we have an approximate dynamical $\mathbb{S}^1$ symmetry whose existence was implied already by Pauli and so it will be called *Pauliean* symmetry. For near-orthogonal fields, the lowest order $\Delta E^{(1)}$ can be written, up to a factor, as $\mu + (d + O(d^2))\nu$, where $d \ll 1$ is called *detuning*. The set of systems near the 1:1 resonance is called the 1:1 zone, see [26].

Normalization of ΔE with respect to μ gives the integrable *second normalized energy correction function* $\Delta\mathcal{E}$. The integrals are the two momenta N and μ,[5] with values n and m respectively, together with $\Delta\mathcal{E}$. Reduction of the 1:1 $\mathbb{S}^1$ symmetry generated by μ defines an 1-DOF Hamiltonian system on the reduced space $P_{n,m}$ (see section 3.3) with Hamiltonian function $\Delta\mathcal{E}$. Note that we denote the second normalized energy correction function on $\mathbb{S}^2 \times \mathbb{S}^2$ and its reduced form on $P_{n,m}$ by the same symbol $\Delta\mathcal{E}$. N, μ are constant on $P_{n,m}$ with values n, m respectively. Finally, from $\Delta\mathcal{E}$ we obtain a simpler Hamiltonian $\mathcal{H}$ by removing the 'constant' (on $P_{n,m}$) terms, i.e., terms that depend only on the dynamical constants n and m. Such terms are not important for the qualitative study of the fibration of the phase space. The value of $\mathcal{H}$ is denoted by h and will be called, for brevity, energy.

1.3. Qualitative characterization of different perturbations

Our analysis is built on the global integrable approximation to the system with Hamiltonian in (1). As explained in section 1.2, and in more detail in section 3, this approximation is obtained by normalization. We study the combined level sets of first integrals: the *energy* $\mathcal{H}$ and the two *momenta* N, μ. We call these sets *fibres*. They may consist of one or several invariant connected components. For each member of the parametric family of systems with Hamiltonian in (1), we describe how fibres 'fit together' in the classical phase space. In mathematics, the entire family of the fibres of the system is described as a *singular Lagrangian fibration* [39]. The base space of the fibration is, by definition, the range of the energy–momentum map

$$\mathcal{EM} = (N, \mu, \mathcal{H}), \tag{6}$$

with values (n, m, h). In our case the range is a domain in $\mathbb{R}^3$. The base space is stratified into sets of regular and critical values of $\mathcal{EM}$. Such stratified range of the $\mathcal{EM}$ map is often called *bifurcation diagram* $\mathcal{BD}$ [39, 40]. This terminology is due to the fact that such diagram shows how the topology of the fibres changes as their image moves in the range of the $\mathcal{EM}$ map. Topologically different diagrams represent qualitatively different fibrations, i.e., qualitatively different perturbations of the hydrogen atom.

Note that the concept of $\mathcal{BD}$ has to be further developed in order to be used in our study. A typical $\mathcal{BD}$ consists of one or several *lower cells* separated by *walls* [26, 41]. Each cell includes regular $\mathcal{EM}$ values and may have an internal structure, such as internal walls or isolated sets of critical values which make it non-simply connected, see figure 2 left. Moreover, a regular $\mathcal{EM}$ value may represent a fibre consisting of several connected components. In such situations we think of the $\mathcal{BD}$ as of a surface with several leaves (or *unfolded lower cells*) where points on each leaf represent single connected components and we *unfold* the stratified $\mathcal{EM}$ range into a covering surface that we call *unfolding surface* or *unfolded* $\mathcal{BD}$ [26]. In our case, such unfolding is needed for systems of type *B* (see table 3); we illustrate it in figure 2(right) and figure 3. The two cells of this surface are glued along a one-dimensional segment of critical $\mathcal{EM}$ values $\mathcal{C}$.

[5] Functions like N and μ that have periodic flows with constant period are called *momenta* or *actions* [38]. Physicists often call actions both the functions and their values.

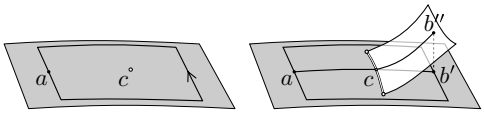

Figure 2. Monodromy of systems with non-simply connected unfolded cells: systems of type A_1 or A_2 (left) and B_1 (right). Point c in the leftmost image is an isolated critical value which lifts to a pinched torus; other points and paths are similar to those in figure 3. Reproduced with permission from [26].

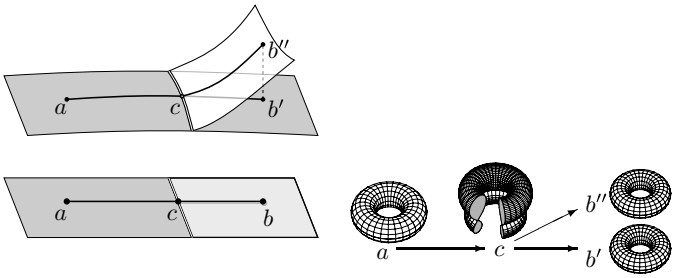

Figure 3. Schematic representation of two overlapping lower cells in the $\mathcal{EM}$ image (bottom left) and the corresponding two-sheet cell unfolding surface (top left) for systems of type B_0 in table 3. Points a, b', b'' and c lift each to a connected component (right); b' and b'' correspond to the same $\mathcal{EM}$ value b. Double line marks branching boundary; bold solid line marks a path connecting a, c and b; corresponding change in the topology of the fibre is illustrated on the right. Reproduced with permission from [26].

1.4. Relation to the quantum mechanical system

Concluding the introduction, we like to point out that this work applies directly to the description of the real quantum atomic system whose classical analogue we study. The relation is provided by the quantum–classical correspondence based on the Einstein–Brillouin–Keller (EBK) quantization principle known also as torus or action quantization. So we invite the reader to keep this relation in mind while going through the necessary details of the analysis based largely on the 'abstract' theory of nonlinear Hamiltonian dynamical systems and corresponding toric fibrations.

In quantum mechanics, we characterize the *lattice* [30, 42] formed within the range of the $\mathcal{EM}$ by the joint spectrum of mutually commuting operators which correspond to the first integrals. We describe the lattice qualitatively and relate this description to that of the classical system by superimposing the lattice on the bifurcation diagram. Its essence again is in considering all states of the system *together*, i.e., for all possible values of energy and momenta, and to characterize the lattice *globally*.

According to the EBK quantization principle, quantum energies correspond to those tori, for which the values of *local* classical actions are integer multiples of $\hbar$ plus a small correction. So the joint quantum spectrum is *locally* isomorphic to a three-dimensional regular orthogonal lattice $\mathbb{Z}^3$ where the distance between adjacent nodes is $\hbar$. In our case the integrals N and μ are globally defined actions, see footnote 5. The energy $\mathcal{H}$ is not an action, because its flow is not periodic. So we have to construct the third action locally. For the quantum system this means that we have two global quantum numbers n and m but the third quantum number may or may not be defined globally. To verify whether a third global number can be defined

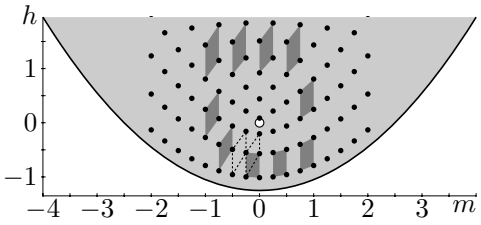

Figure 4. The joint spectrum for the 1:(−1) resonance. The nontriviality (defect) of the lattice can be uncovered through parallel transport of an elementary cell; it corresponds to monodromy 1.

we consider a three-dimensional *elementary cell*, i.e., a volume element defined by adjacent points in the joint spectrum, and *parallel transport* it along a closed path in the connected domain of regular $\mathcal{EM}$ values. If for all closed paths the cell comes to itself after making one tour then it is possible to define such global number therefore our lattice is just a deformed $\mathbb{Z}^3$ lattice.

The situation becomes more interesting when we have a non-simply connected set of regular $\mathcal{EM}$ values. In this case the system has monodromy. As a consequence, no smooth action coordinates can be globally defined. The corresponding joint spectrum is not a regular lattice. Instead it can be described as a lattice with one or more elementary defects, see [42]. Recall from section 1.3 that we may have several connected sets of regular $\mathcal{EM}$ values. In such situations we do the above construction within each connected set (unfolded lower cell).

A simple example that is relevant to the hydrogen atom is the 1:(−1) resonance system [41, 43]. This system has an unstable focus–focus equilibrium, which is represented by the isolated critical energy–momentum value (0, 0) in figure 4. Also shown in this figure is an elementary cell which is parallel transported around (0, 0) and which does not come back to itself after making one tour. So the lattice in figure 4 has a defect. We will observe exactly the same behaviour in the perturbed hydrogen atom.

Note that there may be other complications of the joint spectrum which are characterized in terms of generalized quantum monodromy (fractional monodromy, bidromy) [41, 43–46]. Such cases do not appear in the present system with near-perpendicular fields but they do appear for other field configurations [26].

1.5. Structure of the paper

The main results of the paper concerning the stratification of the 1:1 zone and the properties of the different types of strata are presented in section 2. In section 3, we give a brief summary of technical results of normalization and reduction which are used to support the statements in section 2. In section 4, we give the basic points of the analysis of the reduced Hamiltonian $\mathcal{H}$ that we use to obtain the $\mathcal{BD}$ of our system and we demonstrate this type of analysis in a particular case. Finally, in section 5 we compute quantum lattices for certain concrete strengths of the perturbing fields and relate them to the classification in section 2. This provides concrete quantum illustrations of the results in section 2.

2. Results: structure of the 1:1 zone

To study all near-orthogonal perturbations with Hamiltonian (1) which constitute the 1:1 zone, we construct the integrable approximation using a detuned 1:1 resonant normal form, as

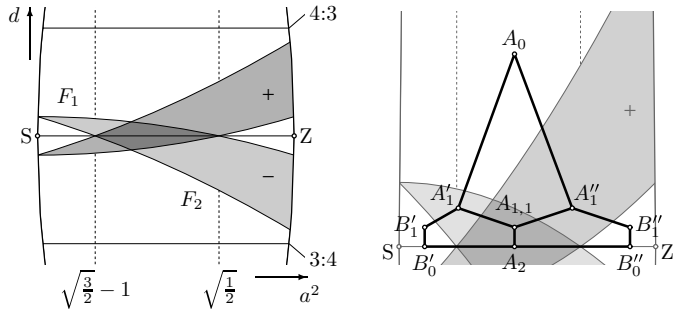

Figure 5. Structure of the 1:1 zone. Different dynamical strata of the zone (left) correspond to vertices of the genealogy graph (right). Vertical edges of the graph represent bifurcations with broken symmetry of order 2, other edges correspond to Hamiltonian Hopf bifurcations.

described in section 3. We use the second order of this normal form to describe the structure of the 1:1 zone. In addition to the idea of the zone [26], two further concepts are essential here, namely the $\mathcal{BD}$ type in the $\mathcal{EM}$ space and the dynamical stratum in the parameter space. Each dynamical stratum contains systems with the same type of $\mathcal{BD}$. Our notation for strata is derived from that of $\mathcal{BD}$ types as will be explained later.

Structurally stable $\mathcal{BD}$ types. The three-dimensional $\mathcal{BD}$ in the space (n, m, h) can be analysed by considering constant n sections $\mathcal{BD}_n$. Such sections correspond to the entire n-shells of the H atom. Table 3 lists all structurally stable $\mathcal{BD}_n$ types that we encounter in the 1:1 zone. Because $\mathcal{BD}_n$ varies piecewise smoothly with n, for any type of $\mathcal{BD}_{n_0}$ in table 3 there is an interval $(n', n'') \ni n_0$ such that all $\mathcal{BD}_n$ with $n \in (n', n'')$ have the same type. In other words, the three-dimensional $\mathcal{BD}$ is locally a cylinder over $\mathcal{BD}_{n_0}$.

The 1:1 zone. In the parameter space—a cylinder in parameters $(s > 0, d, a^2)$—the exact 1:1 resonance corresponds to $d = 0$ and the extent of the detuning is given by $|d|$. The range of the validity of the detuned 1:1 resonant normal form can be given by the inequality [26]

$$|d| \leqslant d_{\max}(s), \qquad \text{where} \quad 0 < d_{\max}(s) \ll \tfrac{1}{2}.$$

After fixing a suitably small $s > 0$, we obtain the parameter disc D with coordinates (d, a^2), where all the systems in the 1:1 resonance zone are represented by a stripe with the line segment $\{d = 0, a^2 \in [0, 1]\}$ in the middle, see figure 5.

Strata. Among these systems, we distinguish several sets which we call *dynamical* and *symmetry action strata*. The symmetry stratification (section 2.1) was originally given in [33, 47]. In this work, we further classify each symmetry stratum into *dynamical* strata, see section 2.2. The equivalence of systems within the same dynamical stratum is defined in section 2 of [26]. The idea there is to study an integrable approximation (normal form) of the system, describe the fibration given by the approximate integrals and compare the $\mathcal{BD}_n$'s for different systems. Within the dynamical stratum, systems should be qualitatively the same, i.e., have the same $\mathcal{BD}_n$'s, and more specifically have the same type of critical fibres and corresponding sets of critical values. As a consequence systems in the same dynamical stratum have the same monodromy, see section 2.3.

Scaling properties. Analysis of the normal form shows that the effective perturbation parameter for the 1:1 zone is (ns). It follows that in order to describe the 1:1 zone we only have to

Table 2. Symmetry strata of the constant s section D_s of the parameter space of the family of perturbations of the hydrogen atom with Hamiltonian in (1), cf figure 5. Dimensionless parameters a^2 and d are defined in (4*a*).

Stratum	Dim	Symmetry	Definition
S	0	$C_{\infty v} \times \mathcal{T}$	$a = 0$
Z	0	$C_{\infty h} \wedge \mathcal{T}_s$	$a = 1$
$\parallel$	1	$C_\infty \wedge \mathcal{T}_s$	$d^2 = a^2(1 - a^2), a^2 \in (0, 1)$
(SZ)	1	$\mathbb{Z}_2 \times \mathcal{T}_s$	$d = 0, a^2 \in (0, 1)$
Generic, G	2	$\mathcal{T}_s$	$0 < d^2 < a^2(1 - a^2), a^2 \in (0, 1)$

consider (ns) instead of n and s individually. As $(ns) \ll 1$ varies, the dynamical stratification of the 1:1 zone remains qualitatively invariant, although the size and shape of different strata in the parameter disc D with coordinates (a^2, d) may change. In particular, the size of the dynamical strata along the d-direction scale almost linearly with (ns), see (7); this property is specific to the 1:1 zone. This implies that knowledge of the dynamical strata, and thus of the possible $\mathcal{BD}_n$ types, for fixed values of n and s gives all possible such types for any other values of n and s.

The scaling properties of the 1:1 system allow us to consider only one constant s section of the parameter space and a fixed value of n for all $\mathcal{BD}_n$'s. Our main result is a complete description of the dynamical strata and the types of $\mathcal{BD}_n$'s in such constant s section. Since we study exclusively constant n sections of the bifurcation diagram, in the following we denote such sections simply $\mathcal{BD}$.

2.1. Symmetry stratification of the 1:1 zone

The systems within each symmetry stratum are invariant with respect to the same symmetry group, see table 2 which summarizes results from [33, 47]. For each symmetry stratum we describe the symmetry group by giving a set of generators.

Systems with only electric field **F** define the zero-dimensional Stark (S) stratum. They have symmetry $C_{\infty v} \times \mathcal{T}$. Here $\mathcal{T}$ is the order 2 group $\{1, T\}$ where T denotes the time reversal operation $(\mathbf{Q}, \mathbf{P}) \to (\mathbf{Q}, -\mathbf{P})$. $C_{\infty v}$ consists of rotations about the axis defined by **F** and reflections through all planes that contain the same axis. For each $s > 0$ the S symmetry stratum is defined by $a^2 = 0, d = 0$.

Systems in the zero-dimensional Zeeman (Z) stratum, i.e., with only magnetic field **G** have symmetry $C_{\infty h} \wedge \mathcal{T}_s$. Here $\mathcal{T}_s$ is the order 2 group $\{1, T_s\}$ where $T_s = T \circ \sigma$ denotes time reversal T and reflection σ through a plane that contains the axis defined by **G**. $C_{\infty h}$ consists of rotations about the axis **G** and reflections σ_h through the plane that is perpendicular to **G** and passes through the origin. The complete symmetry group is obtained by combining (denoted by $\wedge$) the generators of the $C_{\infty h}$ and $\mathcal{T}_s$ groups. The defining equations of the Z stratum are $a^2 = 1$ and $d = 0$.

The one-dimensional parallel ($\parallel$) stratum has symmetry $C_\infty \wedge \mathcal{T}_s$, i.e., the same as Z stratum except reflections σ_h. The $\parallel$ stratum is defined by $d^2 = a^2(1 - a^2)$ and $a^2 \in (0, 1)$.

Systems with perpendicular electric and magnetic fields form the one-dimensional (SZ) stratum defined by $d = 0$ and $a^2 \in (0, 1)$. Such systems have discrete symmetry $\mathbb{Z}_2 \times \mathcal{T}_s$ of order 4, where $\mathbb{Z}_2 = \{1, \sigma_h\}$.

Finally, all the other systems form a two-dimensional *generic* symmetry stratum G. Their residual symmetry is the order 2 group $\mathcal{T}_s$.

2.2. Dynamical stratification of the 1:1 zone

First we describe two-dimensional dynamical strata in the parameter space D. Such strata belong in the generic symmetry stratum and they are open in D. Therefore they represent structurally stable systems. Since the structure of the zone is symmetric with respect to the reflection $d \mapsto -d$, we consider only the strata in the positive semidisc $D_+ = D \cap \{d > 0\}$. For $(a^2, d) \in D_+$ the two-dimensional dynamical strata are defined with the help of the functions

$$F_1(a^2) = \tfrac{1}{4}(1 - 2a^4)(ns) + O(ns)^3, \tag{7a}$$

$$F_2(a^2) = \tfrac{1}{4}(1 - 4a^2 - 2a^4)(ns) + O(ns)^3, \tag{7b}$$

and they are (see figure 5)

$$\begin{aligned}
A_1' &= \{|F_2(a^2)| < d < F_1(a^2)\},\\
A_1'' &= \{|F_1(a^2)| < d < -F_2(a^2)\},\\
A_{1,1} &= \{0 < d < \min(F_1(a^2), -F_2(a^2))\},\\
B_1' &= \{0 < d < F_2(a^2)\},\\
B_1'' &= \{0 < d < -F_1(a^2)\},\\
A_0 &= \{\max(F_1(a^2), -F_2(a^2)) < d < d_{\max}\}.
\end{aligned} \tag{8a}$$

Their notation is derived from the type of their $\mathcal{BD}$ given in table 3. Some two-dimensional strata in D_+ consist of several connected components. The components near the Stark and Zeeman configurations are marked respectively by $'$ and $''$, see figure 5. For example systems in the A_1' and A_1'' dynamical strata have $\mathcal{BD}$'s of type A_1. Note that in figure 5 the $A_{1,1}$ stratum is shaded dark grey, the A_1 strata are shaded grey and the rest are left white. All these dynamical strata persist under small deformations of the Hamiltonian. Thus we still find them if we consider higher-order terms of the normalized Hamiltonian.

The boundary of each two-dimensional dynamical stratum is a union of one- and zero-dimensional dynamical strata. Among those we consider only the dynamical strata that are characterized by specific symmetries and therefore persist for all orders of the normalized Hamiltonian.

The zero-dimensional dynamical strata S and Z are defined entirely by their symmetry, i.e., they coincide with the symmetry strata S and Z described in section 2.1. Both lie in the 1:1 zone. The respective Stark and Zeeman systems have been studied historically first. The S stratum is dynamically unique, i.e., its $\mathcal{BD}$ is different from that of neighbouring systems in the generic and (SZ) symmetry strata. Although the Z stratum is distinguished by symmetry, it has the bifurcation diagram of the type B_0 (see table 3), just as the neighbouring systems in the dynamical stratum B_0''.

The one-dimensional $(SZ) \subset D$ symmetry stratum belongs entirely in the 1:1 zone. It is further dynamically stratified into three one-dimensional parts,

$$\begin{aligned}
B_0' &= \{d = 0, 0 < a^2 < \sqrt{3/2} - 1\},\\
A_2 &= \{d = 0, \sqrt{3/2} - 1 < a^2 < \sqrt{1/2}\},\\
B_0'' &= \{d = 0, \sqrt{1/2} < a^2 < 1\}.
\end{aligned} \tag{8b}$$

Near S and Z, the 1:1 zone also includes the parts of the symmetry stratum $\|$ which are also further stratified dynamically. For $(a^2, d) \in \partial D_+$ (the upper half of the $\|$ symmetry stratum)

Table 3. Qualitatively different $\mathcal{BD}$'s of systems in the 1:1 zone. In the second column we show a constant-n section of the bifurcation diagram. The horizontal and vertical axes of $\mathcal{BD}$'s represent m and h respectively. In the fourth and fifth columns we give the symmetry and dynamical strata respectively that contain systems with the given $\mathcal{BD}$, see also figure 5. In the fourth column the symbol G stands for the generic stratum, see section 2.1. The dynamical strata are defined in section 2.2. Monodromy is described in detail in section 2.3.

$\mathcal{BD}$ type	$\mathcal{BD}_n$	Comments	Symm. strata	Dyn. strata
A_0		The $\mathcal{BD}$ consists of a single lower cell. Trivial monodromy.	G, $\parallel$	A_0, $\parallel A_0'$, $\parallel A_0''$
A_1		The $\mathcal{BD}$ contains one isolated critical value o that corresponds to a simply pinched torus $\mathbb{T}^2_{[1]} \times \mathbb{S}^1$. Non-trivial monodromy.	G, $\parallel$	A_1', A_1'', $\parallel A_1''$
$A_{1,1}$		The $\mathcal{BD}$ contains two isolated critical values o^-, o^+ that correspond to simply pinched tori $\mathbb{T}^2_{[1]} \times \mathbb{S}^1$. Non-trivial monodromy.	G	$A_{1,1}$
A_2		The $\mathcal{BD}$ contains an isolated critical value o that corresponds to a doubly pinched torus $\mathbb{T}^2_{[2]} \times \mathbb{S}^1$. Non-trivial monodromy.	(SZ)	A_2
B_1	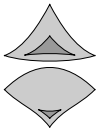	The unfolded $\mathcal{BD}$ contains two partially overlapping unfolded lower cells glued along a line. Non-trivial monodromy. Both $\mathcal{BD}$'s depicted here are equivalent. The top appears in the B_1' dynamical stratum and the bottom in the B_1'' and $\parallel B_1''$ dynamical strata.	G, $\parallel$	B_1', B_1'', $\parallel B_1''$
B_0	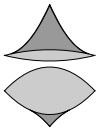	The unfolded $\mathcal{BD}$ consists of three unfolded lower cells glued along a line; two of the cells overlap completely (dark shade). Trivial monodromy. Both $\mathcal{BD}$'s depicted here are equivalent. The top appears in B_0' and the bottom in the B_0'' and Z dynamical strata.	(SZ), Z	B_0', B_0'', Z
A_0^*		The unfolded $\mathcal{BD}$ consists of one unfolded lower cell that partially self overlaps. Trivial monodromy. Unfolding a $\mathcal{BD}$ of type A_0^* gives a $\mathcal{BD}$ of type A_0.	$\parallel$	$\parallel A_0^*$
S		The unfolded $\mathcal{BD}$ consists of one unfolded lower cell that self-overlaps. Trivial monodromy. This is a special case of A_0^* with extra $\mathbb{Z}_2$ symmetry.	S	S

we have the following dynamical strata:

$$\begin{aligned}
\parallel A_0^* &= \{(a^2, d) \in \partial D_+, 0 < d < F_2(a^2), a^2 < 1/2\},\\
\parallel A_0' &= \{(a^2, d) \in \partial D_+, F_1(a^2) < d < d_{\max}, a^2 < 1/2\},\\
\parallel A_0'' &= \{(a^2, d) \in \partial D_+, |F_2(a^2)| < d < d_{\max}, a^2 > 1/2\},\\
\parallel A_1'' &= \{(a^2, d) \in \partial D_+, |F_1(a^2)| < d < |F_2(a^2)| a^2 > 1/2\},\\
\parallel B_1'' &= \{(a^2, d) \in \partial D_+, 0 < d < |F_1(a^2)|, a^2 > 1/2\},
\end{aligned} \tag{8c}$$

2.3. Topology of $\mathcal{BD}$ and monodromy

The most important qualitative difference between the different types of $\mathcal{BD}$'s in table 3 is the existence of different unfolded lower cells. Further difference can be given by the topology of each cell, notably whether it is simply connected or not, and by the nature of the critical values involved and the respective critical fibres. The torus bundle over the regular interior of a non-simply connected cell has nontrivial monodromy. This makes monodromy an important characteristic of the cell.

A_0 systems are the most simple: within their bifurcation diagram, the image of the set of all regular tori (shaded grey in table 3) is simply connected. These systems have no monodromy and can be described using global action–angle variables. Other systems with global action–angle variables but with more complicated $\mathcal{BD}$'s are B_0, A_0^* and S. The A_1, $A_{1,1}$, A_2 and B_1 systems have monodromy of different kinds described here.

2.3.1. Cycle bases on regular tori. Recall that the integrable approximation of the original Hamiltonian constructed after two normalizations has two integrals N and μ. The corresponding Hamiltonian vector fields X_N and X_μ have 2π periodic flows, hence N and μ are two actions (see footnote 5). A third action I_3 can be constructed (locally) using the flow of $X_\mathcal{H}$. This construction is, basically, Cushman's method [48] with modifications detailed in [34]. The flows of the corresponding vector fields X_N, X_μ and X_{I_3} define homology cycles γ_N, γ_μ and γ_3 respectively on the regular tori $\Lambda_{n,m,h} = \mathbb{T}^3$ corresponding to specific regular value (n, m, h) of $\mathcal{EM}$ (6). These cycles form a basis of the first homology group $H_1(\Lambda_{n,m,h}, \mathbb{Z})$. Note that the values of actions N, μ and I_3 are obtained by integrating $\mathbf{P}d\mathbf{Q}$ along the respective cycles γ_N, γ_μ and γ_3.

2.3.2. General statement on monodromy. We compute monodromy by continuing explicitly cycles γ_N, γ_μ and γ_3 along closed paths Γ in the connected set of regular values R of the $\mathcal{EM}$ map within an unfolded lower cell of the $\mathcal{BD}$. After a tour on Γ the cycle basis may change. The map between the initial and the final cycle bases characterizes monodromy. For concrete basis choices this map is given by a matrix in $\mathrm{SL}(3, \mathbb{Z}) \subset \mathrm{GL}(3, \mathbb{Z})$ which is called the *monodromy matrix*[6].

Because, as explained before, our three-dimensional bifurcation diagram is locally a cylinder in n, it is enough to consider constant n closed paths, i.e., closed paths that lie on constant n sections $\mathsf{R}_n \subseteq \mathcal{BD}_n$. The novelty with respect to previous work [26–28] is that we compute the monodromy matrix for the three-dimensional $\mathcal{EM}$ map and we confirm by this computation that the Keplerian cycle γ_N does not participate in the monodromy transformation expressed in the basis $(\gamma_N, \gamma_\mu, \gamma_3)$ of $H_1(\Lambda_{n,m,h}, \mathbb{Z})$.

For a given closed path Γ monodromy may be nontrivial only if Γ cannot be contracted to a point inside R. This occurs for types A_2, $A_{1,1}$, A_1 and B_1. In all these cases, we can choose a closed path $\Gamma \subset \mathsf{R}_n$ which encircles an isolated set of critical values. Monodromy is the same for any Γ in the homotopy class $[\Gamma]$.

The actions N and μ define cycles γ_N and γ_μ, respectively, that depend smoothly on $(n, m, h) \in \mathsf{R}$. These cycles remain unchanged as we go along Γ. The third basis cycle γ_3 of $H_1(\Lambda_{n,m,h}, \mathbb{Z})$ transforms after completing a tour along Γ as

$$\gamma_3 \mapsto \gamma_3 - \mathbf{k} \cdot (\gamma_N, \gamma_\mu) = \gamma_3 - k_N \gamma_N - k_\mu \gamma_\mu.$$

[6] The *group* $\mathrm{GL}(3, \mathbb{Z})$ consists of all 3×3 integer matrices with determinant ± 1. Although in general the monodromy matrix is an element of $\mathrm{GL}(3, \mathbb{Z})$, in our study we encounter only monodromy matrices in $\mathrm{SL}(3, \mathbb{Z})$, i.e., with determinant +1.

Table 4. Monodromy matrix $M(\mathbf{k})$ (see (9) for $\mathbb{T}^3 \subset \mathbb{R}^6$ in systems of different strata (cf table 3). For systems of type $A_{1,1}$ we distinguish additionally monodromy matrices corresponding to the circuits $[\Gamma^+]$, $[\Gamma^-]$ and $[\Gamma^-]+[\Gamma^-]$ which go around the two distinct isolated critical values with $m = 0$, the upper o^+ and the lower o^-, and around both values, respectively (see figure 6). The three cases are denoted by $A^+_{1,1}$, $A^-_{1,1}$ and $A^{+-}_{1,1}$.

System, case	k_μ	k_N
A_2, $A^{+-}_{1,1}$	2	0
$A^+_{1,1}$, A'_1, B'_1	1	0
$A^-_{1,1}$, A''_1, B''_1	1	0

This transformation is characterized by two integers k_μ and k_N and therefore in the basis $\{\gamma_N, \gamma_\mu, \gamma_3\}$ the 3×3 monodromy matrix is

$$M_{[\Gamma]} = \begin{pmatrix} 1 & 0 & 0 \\ 0 & 1 & 0 \\ -k_N & -k_\mu & 1 \end{pmatrix}. \tag{9}$$

The values of k_μ and k_N for systems in different dynamical strata are given in table 4. We observe that $k_N = 0$ and so γ_N is not involved in the transformation expressed in the chosen basis. The matrix for 1:1 systems is $\mathrm{diag}(1, M(k))$ with the 2×2 block $M(k)$ of the form

$$M(k) = \begin{pmatrix} 1 & 0 \\ -k & 1 \end{pmatrix} \tag{10}$$

and $k = k_\mu$ equal to either 1 or 2.

2.3.3. Monodromy in specific cases. In both cases A_1 and A_2, $\mathcal{BD}_n$ consists of one cell with one isolated critical $\mathcal{EM}_n$-value o inside. The set of regular values is not simply connected, and we consider monodromy for a nontrivial closed path Γ that goes once around o, see figure 2, left. In the case of A_2 which was studied early in [4], o corresponds in $\mathbb{S}^2 \times \mathbb{S}^2$ to a doubly pinched torus $\mathbb{T}^2_{[2]}$, see figure 7. This implies by the geometric monodromy theorem [21, 23] that the A_2 system has nontrivial monodromy with $k = 2$. In the case A_1, the isolated critical value o lifts to a singly pinched torus $\mathbb{T}^2_{[1]}$ in $\mathbb{S}^2 \times \mathbb{S}^2$ (figure 7) and $k = 1$. We confirmed this by explicit cycle construction [34].

The B_1 systems can be obtained as a deformation of A_1. The B_1 type $\mathcal{BD}_n$ consists of two partially overlapping cells that join along a curved segment $\mathcal{C}$ of critical values. The corresponding cell unfolding surface is shown schematically in figure 2, right. The critical segment $\mathcal{C}$ is isolated in the 'larger' cell, and is part of the boundary of the 'smaller' cell. The latter can be deformed continuously together with $\mathcal{C}$ into a single isolated critical value of the A_1 system. Under such deformation, the circuit Γ that goes around the segment in the set of regular values of the larger cell (figure 2, right) transforms continuously into the circuit Γ of the A_1 case (figure 2, left). Hence $k = 1$, and the monodromy of B_1 is the same as that of A_1.

In the case of the $A_{1,1}$ systems, the $\mathcal{BD}_n$ has two isolated critical values o^- (lower in h) and o^+ (higher in h), each lifting to a singly pinched torus $\mathbb{T}^2_{[1]}$ in $\mathbb{S}^2 \times \mathbb{S}^2$. The fundamental group of the $A_{1,1}$ type $\mathcal{BD}_n$ has two nontrivial cycles $[\Gamma^-]$ and $[\Gamma^+]$ represented in figure 6, top right, by closed paths Γ^- and Γ^+ encircling o^- and o^+, respectively. We compute $k^- = k^+ = 1$ which agrees both with the 'sign' theorem [49] and the geometric monodromy theorem. We compute that both matrices $M_{[\Gamma^-]}$ and $M_{[\Gamma^+]}$ are of the type in (10) with $k^- = k^+ = 1$.

The monodromy map is a homomorphism $[\Gamma] \to M_{[\Gamma]}$ so the monodromy map for the circuit $[\Gamma] = [\Gamma^-] + [\Gamma^+]$ that goes once around both critical values (see figure 6, top right)

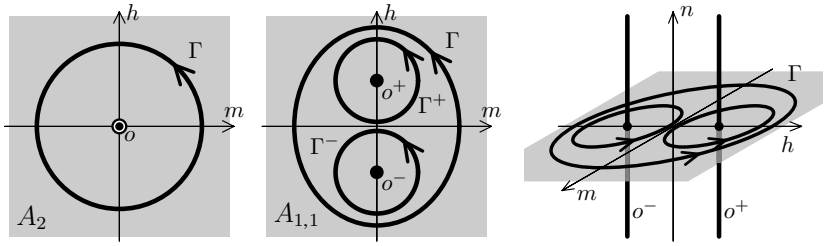

Figure 6. The image of the energy–momentum map $\mathcal{EM}$ in (6) defined by first integrals $(N, \mu, \mathcal{H})$ with values (n, m, h). The left and centre pictures show constant-n sections; the three-dimensional image is represented on the right; grey shade represents regular $\mathcal{EM}$ values with the same n. Contour Γ goes around the isolated critical value o, which lifts to a doubly pinched torus (left) of an A_2 system, and around two isolated critical values o^- and o^+, each lifting to a singly pinched torus (centre) of the $A_{1,1}$ system; contours Γ^- and Γ^+ encircle o^- and o^+ respectively. In the full image (right), o, o^- and o^+ become one-dimensional threads of critical values.

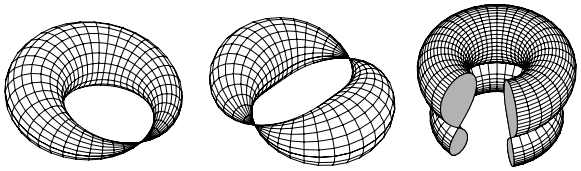

Figure 7. Possible three-dimensional representations of singular fibres in two degree of freedom systems. From left to right, singly pinched torus $\mathbb{T}^2_{[1]}$, doubly pinched torus $\mathbb{T}^2_{[2]}$ and bitorus $\mathbb{T}^2_{\text{bi}}$.

has $k = 2$. The latter result follows also immediately, once we observe that $A_{1,1}$ systems are a deformation of A_2 (see figures 5 and 6, top left).

In the case B_0, also studied in [4], the $\mathcal{BD}$ consists of three unfolded lower cells, two of which overlap. The unfolded $\mathcal{BD}$ is illustrated in figure 3. The regular interior of each cell is simply connected. There is no monodromy.

2.4. Bifurcations in the 1:1 zone

We now describe how the strata fit together within the 1:1 zone, see figure 5. This can be done as follows: there is a number of open (in their symmetry stratum), connected, non-intersecting sets whose mutual position within the zone can be specified by a system of typical paths. This makes up the graph in figure 5 (right). The vertices of the graph represent the sets and the edges represent the paths. As we go along each path we should expect one or several bifurcations to happen. From the structural point of view, going from the centre of the zone towards $|d| = d_{\max}$ results in simplification so that arriving at the A_0 stratum indicates the periphery of the zone.

Along the paths $A_2 \to A_{1,1}$, $B_0' \to B_1'$ and $B_0'' \to B_1''$ the specific $\mathbb{Z}_2$ symmetry of the orthogonal configuration breaks. Along all the other paths the system goes through a Hamiltonian Hopf bifurcation [50]. Along the paths $B_1' \to A_1'$ and $B_1'' \to A_1''$ the system goes through a subcritical Hamiltonian Hopf bifurcation. In such bifurcation an elliptic periodic orbit is attached to a family of $\mathbb{T}^2$. The family shrinks and at the bifurcation it vanishes while the periodic orbit becomes unstable (generically complex hyperbolic unless there is extra symmetry).

Along the paths $A_1' \to A_{1,1}$, $A_1'' \to A_{1,1}$, $A_0 \to A_1'$ and $A_0 \to A_1''$ the system goes through a supercritical Hamiltonian Hopf bifurcation. In such bifurcation an elliptic periodic orbit is again attached to a family of $\mathbb{T}^2$. At the bifurcation the periodic orbit detaches from the family of $\mathbb{T}^2$ and becomes unstable.

Finally, along the paths $B_0' \to A_2$ and $B_0'' \to A_2$ the system goes through Hamiltonian Hopf bifurcations that are degenerate at the order of truncation of the normal form used in this work. These degenerate bifurcations have been resolved in [25] where it was shown that one of them is subcritical and the other supercritical.

The $\|$ stratum requires a special comment. Systems at the Z side are dynamically indistinguishable from nearby systems outside the $\|$ stratum. At the S side the situation near and in S appears to be degenerate and considering higher-order terms in the normal form may change this picture. As we move away from S, systems in the $\|A_0^*$ dynamical stratum are dynamically distinct from systems in the neighbouring B_1' stratum. They are A_0 type systems with a folded $\mathcal{BD}$. Next comes the $\|A_0'$ stratum near the boundary of the 1:1 zone.

3. Technical results

In this section, we obtain an integrable approximation to the system with the Hamiltonian in (1). After reduction we obtain an 1-DOF Hamiltonian system with Hamiltonian $\mathcal{H}$ on the reduced phase space $P_{n,m}$. For $m \neq 0, \pm n$, the space $P_{n,m}$ is a smooth sphere, for $m = 0$ it is a topological sphere with two singular points and finally for $m = \pm n$ it is a point. Our further analysis is based on $\mathcal{H}$ for which the parameter space is described using n-scaled fields. This differs from previous work [4, 25, 26] where the analysis was based on energy-scaled fields.

3.1. Normalization and reduction of the Keplerian symmetry

The first step in the construction is the Kustaanheimo–Stiefel (KS) regularization of the singularity of the Keplerian potential through which the system with Hamiltonian H_{3D} in (1) is described as a Hamiltonian system in $\mathbb{R}^8$ with Hamiltonian H_{KS}. The KS Hamiltonian H_{KS} is normalized and reduced with respect to its unperturbed part $2N$, see [4].

The specifics of the KS method is that the physical energy E now enters in the formal smallness parameter of the series for the normalized KS Hamiltonian H_{KS} while the value of the latter is a fictitious constant. Then the first normalized energy $E(\mathbf{X}, \mathbf{Y})$ can be obtained by the normalized H_{KS} using formal series inversion as detailed in [34], see also section 5.1 of [4] and earlier work [51]. These steps of the procedure are detailed in [4, 34]. The first normalized energy is expressed in terms of the *Pauli* vectors

$$(\mathbf{X}, \mathbf{Y}) = (X_1, X_2, X_3, Y_1, Y_2, Y_3) \tag{11}$$

that satisfy

$$X_1^2 + X_2^2 + X_3^2 = Y_1^2 + Y_2^2 + Y_3^2 = \frac{n^2}{4}. \tag{12}$$

Note that the vectors $\mathbf{L} = \mathbf{X} + \mathbf{Y}$ and $\mathbf{K} = \mathbf{X} - \mathbf{Y}$ are the KS-transformed angular momentum and Laplace–Runge–Lenz (or eccentricity) vectors respectively. Equation (12) shows that the reduced phase space is $\mathbb{S}^2 \times \mathbb{S}^2$. The components of $(\mathbf{X}, \mathbf{Y})$ span the Poisson algebra $so(3) \times so(3) \cong so(4)$ so that

$$\{X_i, X_j\} = \sum_{k=1}^{3} \varepsilon_{ijk} X_k, \qquad \{Y_i, Y_j\} = \sum_{k=1}^{3} \varepsilon_{ijk} Y_k, \qquad \{X_i, Y_j\} = 0. \tag{13}$$

The resulting expression for the energy can be written as

$$E(\mathbf{X}, \mathbf{Y}) = -\frac{1}{2n^2} + \frac{1}{2n^2}\Delta E(\mathbf{X}, \mathbf{Y}), \tag{14}$$

where

$$\Delta E(\mathbf{X}, \mathbf{Y}) = \Delta E^{(1)}(\mathbf{X}, \mathbf{Y}) + \Delta E^{(2)}(\mathbf{X}, \mathbf{Y}) + \cdots \tag{15a}$$

is called the *energy correction function* and each $\Delta E^{(k)}$ contains only terms of degree k both in (f_e, f_b, g) and in $(n, \mathbf{X}, \mathbf{Y})$. The first- and second-degree terms in (15*a*) are respectively,

$$\Delta E^{(1)}(\mathbf{X}, \mathbf{Y}) = (-f_b + g)X_1 - f_e X_2 + (f_b + g)Y_1 + f_e Y_2, \tag{15b}$$

and

$$\begin{aligned}\Delta E^{(2)} = {} & \tfrac{1}{72}\left(9g^2n^2 - 17f_e^2 - 17f_b^2\right)n^2 + \tfrac{1}{6}f_e^2\left(X_2^2 + Y_2^2 + Y_2X_2\right) \\ & + \tfrac{1}{6}f_b^2\left(X_1^2 + Y_1^2 + X_1Y_1\right) + \tfrac{1}{3}g f_e(X_2Y_1 - X_1Y_2) \\ & + \tfrac{1}{6}f_b f_e(2(X_1X_2 + Y_1Y_2) + X_1Y_2 + X_2Y_1) \\ & + \tfrac{1}{2}g^2(X_1Y_1 + (X_2 - Y_2)^2 + (X_3 - Y_3)^2).\end{aligned} \tag{15c}$$

We should further note that the form of the normalized $E(\mathbf{X}, \mathbf{Y})$ is not unique. In the Lie series normalization procedure [52, 53] the generator of the normalization transformation may be modified by adding terms that commute with N and contribute to $\Delta E^{(k)}$, for $k \geqslant 2$. Such terms do not modify the physical results that we obtain later.

3.2. Standard form of the linear term and resonances

In order to simplify further the first-order energy correction term $\Delta E^{(1)}$, in (15*b*), we rotate separately each sphere in $\mathbb{S}^2 \times \mathbb{S}^2$ so that $\Delta E^{(1)}$ becomes a linear combination only of the new coordinates x_1 and y_1. Such rotations are given by

$$\mathbf{X} \mapsto A_-^{-1}\mathbf{x}, \qquad \mathbf{Y} \mapsto A_+^{-1}\mathbf{y}, \tag{16}$$

where

$$A_\pm = \frac{1}{\omega_\pm}\begin{pmatrix} g \pm f_b & \pm f_e & 0 \\ \mp f_e & g \pm f_b & 0 \\ 0 & 0 & \omega_\pm \end{pmatrix}, \tag{17}$$

and

$$\omega_\pm = \sqrt{(g \pm f_b)^2 + f_e^2} = s\sqrt{1 \pm 2d}. \tag{18}$$

Because of the particular form of the transformation (16) the components of $(\mathbf{x}, \mathbf{y})$ satisfy again

$$x_1^2 + x_2^2 + x_3^2 = y_1^2 + y_2^2 + y_3^2 = \frac{n^2}{4}, \tag{19}$$

and the Poisson structure is preserved,

$$\{x_i, x_j\} = \sum_{k=1}^{3}\varepsilon_{ijk}x_k, \qquad \{y_i, y_j\} = \sum_{k=1}^{3}\varepsilon_{ijk}y_k, \qquad \{x_i, y_j\} = 0. \tag{20}$$

In the new variables

$$\Delta E^{(1)}(\mathbf{x}, \mathbf{y}) = \omega_- x_1 + \omega_+ y_1, \tag{21}$$

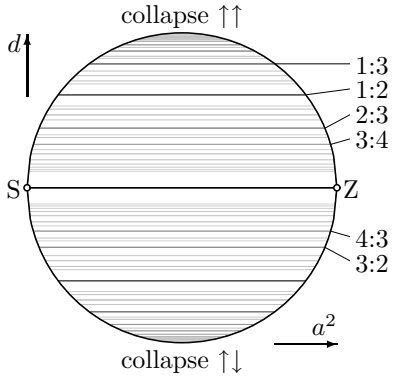

Figure 8. Systems with $k_- : k_+$ resonances in the constant s section (left) of the set of all possible perturbations of the hydrogen atom by static electric and magnetic fields **F** and **G**.

and $\Delta E^{(2)}(\mathbf{x}, \mathbf{y})$ can be computed from (15*c*). Note that $\Delta E^{(k)}$ are homogeneous polynomials of degree k in $(n, \mathbf{x}, \mathbf{y})$ and also in the parameters (f_e, f_b, g). The whole energy correction ΔE is a perturbation of $\Delta E^{(1)}$.

The flow generated by $\Delta E^{(1)}$ on $\mathbb{S}^2 \times \mathbb{S}^2$ is a simultaneous rotation of the two spheres around the axes x_1 and y_1 with frequencies ω_- and ω_+ respectively,

$$t, (x, y) \mapsto (M(\omega_- t)x, M(\omega_+ t)y), \tag{22a}$$

where

$$M(t) = \begin{pmatrix} 1 & 0 & 0 \\ 0 & \cos t & \sin t \\ 0 & -\sin t & \cos t \end{pmatrix}. \tag{22b}$$

The ratio of the frequencies is

$$\frac{\omega_-}{\omega_+} = \sqrt{\frac{1-2d}{1+2d}}, \tag{23}$$

so in the parameter disc D_s each frequency ratio is represented by a horizontal line with fixed d, see figure 8. In the case of perpendicular fields we have $d = 0$ and the ratio is 1:1, i.e., $k_+\omega_- - k_-\omega_+ = 0$ with $k_+ = k_- = 1$. In figure 8 this corresponds to the line (SZ).

As we already mentioned in the introduction, the presence of resonances $k_- : k_+$ is of primary importance to the rest of this study and to the understanding of the system. The subsequent normalization step depends on the particular resonance. So different resonances have to be studied using different normal forms. When we detune the resonance, that is when we move away in D_s from the exact value of d corresponding to the resonance, the latter remains still important provided that the detuning is small. As long as this is the case we remain in what is called in [26] the resonance zone. The 1:1 resonance zone is the largest and thus the most important.

3.3. Normalization and reduction of the residual dynamical symmetry

The energy correction function $\Delta E(\mathbf{x}, \mathbf{y})$ is a Hamiltonian function defined on $\mathbb{S}^2 \times \mathbb{S}^2$. It describes our system for fixed n and different values of E. This is a 2-DOF Hamiltonian system which is in general not integrable. In order to obtain a completely integrable approximation

Table 5. Coefficients of the second-order term $\Delta\mathcal{E}^{(2)}$ in the second reduced energy correction function $\Delta\mathcal{E}$ (29). In the second reduced system $\mu = m$ is a parameter. To represent invariants μ, ν and π_1 as functions on the first reduced space $\mathbb{S}^2 \times \mathbb{S}^2$ use (25). Relation of dimensionless parameters a^2 and d, and smallness parameter s to the electric and magnetic field strengths is given in (2) and (4*a*).

Monomial	Coefficient $\times\, 24s^{-2}(1-4d^2)^{3/2}$
n^2	$a^{-2}(1-4d^2)^{1/2}((2a^2+7)a^4 - 68d^4 + (-36a^4+2a^2+17)d^2)$
μ^2	$((1-4d^2)^{1/2}(-6a^4+(8d^2+4)a^2+22d^2-7) - 10(a^2+2d^2-1)(4d^2-1))$
ν^2	$(10(a^2+2d^2-1)(4d^2-1) + (1-4d^2)^{1/2}(-6a^4+(8d^2+4)a^2+22d^2-7))$
$\mu\nu$	$-24d(1-4d^2)^{1/2}(a^4-a^2+5d^2-1)$
π_1	$3(a^2(1-4d^2)^{1/2}+a^2-2d^2)(4d^2-1)$

we need one more integral which we obtain by normalizing ΔE. Since the near-orthogonal systems that we study are close to the 1:1 resonance we choose to normalize ΔE with respect to the generator $\mu = x_1 + y_1$ of the 1:1 $\mathbb{S}^1$ symmetry (22*a*). In this way, the 1:1 resonant terms that remain important for detuned systems are included in the normal form.

The result of the normalization with respect to the 1:1 resonant $\mathbb{S}^1$ action of μ is a 2-DOF Hamiltonian system on $\mathbb{S}^2 \times \mathbb{S}^2$ with Hamiltonian function

$$\Delta\mathcal{E}(\mathbf{x},\mathbf{y}) = \Delta\mathcal{E}^{(1)}(\mathbf{x},\mathbf{y}) + \Delta\mathcal{E}^{(2)}(\mathbf{x},\mathbf{y}), \tag{24}$$

which we call *second normalized energy correction function*, and where $\Delta\mathcal{E}^{(1)} = \omega_- x_1 + \omega_+ y_1$ is the same as $\Delta E^{(1)}$, and the coefficients of terms in $\Delta\mathcal{E}^{(2)}$ can be deduced from table 5. Because $\{\Delta\mathcal{E}, \mu\} = 0$ this is a Liouville integrable system with exact integrals μ and $\Delta\mathcal{E}$.

The final step in the construction of the integrable approximation for the hydrogen atom in near-orthogonal fields is the reduction of the second normal form $\Delta\mathcal{E}$. For fixed $N = n$, $\mu = m$ this brings us to a 1-DOF system on two-dimensional compact phase space $P_{n,m}$ which we call *second reduced phase space*. We use invariant theory and we follow [4] with some changes in notation[7].

The ring of polynomials in (x, y) invariant under the 1:1 $\mathbb{S}^1$ (22*a*) action is generated by the invariants

$$\begin{aligned} &\nu = x_1 - y_1, && \mu = x_1 + y_1, \\ &\pi_1 = 4(x_2y_2 + x_3y_3), && \pi_2 = 4(x_3y_2 - x_2y_3), \\ &\pi_3 = 4\big(x_2^2 + x_3^2\big), && \pi_4 = 4\big(y_2^2 + y_3^2\big), \end{aligned} \tag{25}$$

that satisfy the (in)equalities

$$\pi_1^2 + \pi_2^2 = \pi_3\pi_4, \qquad \pi_3 \geqslant 0, \quad \text{and} \quad \pi_4 \geqslant 0. \tag{26}$$

From (19) we obtain further that

$$\pi_3 = n^2 - (\nu+\mu)^2, \qquad \pi_4 = n^2 - (\nu-\mu)^2. \tag{27}$$

The relations (26), (27) define the second reduced phase space $P_{n,m}$ for fixed $\mu = m$ such that $|m| \leqslant n$. The space $P_{n,m}$ is the semi-algebraic variety defined by

$$\pi_1^2 + \pi_2^2 = (n^2 - (\nu+m)^2)(n^2 - (\nu-m)^2), \qquad \nu \in [-n + |m|, n - |m|], \tag{28}$$

which can be immersed in the ambient space $\mathbb{R}^3$ with coordinates (ν, π_1, π_2), and projected on the plane (ν, π_1) as depicted in figure 9 for different values of m. Note that $P_{n,m}$ and $P_{n,-m}$

[7] The invariants $(\pi_1, \ldots, \pi_6)$ in [4] are denoted here by $(\nu, \pi_1, \pi_2, \mu, \pi_3, \pi_4)$ respectively.

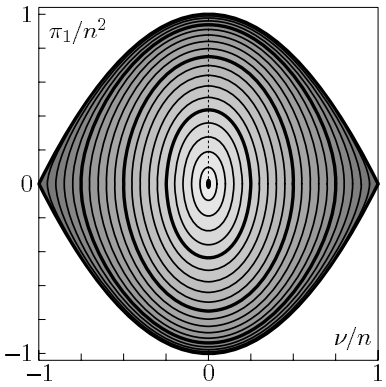

Figure 9. Projections of the reduced phase spaces $P_{n,m}$ to the plane $\{\pi_2 = 2\}$ with coordinates (ν, π_1) for $m = 0$ (outmost boundary), $0 < |m| < n$ (intermediate smooth boundaries) and $m = \pm n$ (point 0). In $\mathbb{R}^3$, each space $P_{n,m}$ is a surface of revolution about the axis ν, so $P_{n,0}$ is a sphere with two singular points, $P_{n,m}$ for $m \neq 0, \pm n$ is a smooth sphere and $P_{n,\pm n}$ are single points, cf figure 3 in [4].

have the same representation. Furthermore, for all values of m the second reduced space $P_{n,m}$ is a surface of revolution around the ν-axis.

The advantage of this construction over any attempts to obtain a reduced space using various action–angle coordinates is that $P_{n,m}$ is a true orbit space and the geometry of the system is preserved. Each smooth point on $P_{n,m}$ lifts to a circle $\mathbb{S}^1$ in $\mathbb{S}^2 \times \mathbb{S}^2$ and consequently to a $\mathbb{T}^2$ in $\mathbb{R}^6$. The singular points on $P_{n,0}$ and the single-point spaces $P_{n,\pm n}$ lift to points on $\mathbb{S}^2 \times \mathbb{S}^2$ and to $\mathbb{S}^1$ orbits in $\mathbb{R}^6$ which are relative equilibria $\mathbb{S}^1$, i.e., periodic orbits $\mathbb{S}^1$ of the Keplerian action. Such orbits are called Kepler ellipses, see [6].

Note that the second reduced system has the residual symmetry $\mathcal{T}_s$ of order 2 (see table 2) that corresponds to the symmetry under the reflection $\pi_2 \mapsto -\pi_2$. Due to this symmetry the second reduced Hamiltonian does not depend on π_2. For this reason it is sufficient to work just with the projection of $P_{n,m}$ on the plane $\{\pi_2 = 0\}$ with coordinates (ν, π_1). This approach was introduced in [4].

Expressing the second normalized energy correction function $\Delta\mathcal{E}$ in (24) in terms of (ν, π_1, π_2) and $\mu = m$ gives the second reduced energy correction function

$$\Delta\mathcal{E}(\nu, \pi_1) = \Delta\mathcal{E}^{(1)}(\nu, \pi_1) + \Delta\mathcal{E}^{(2)}(\nu, \pi_1), \tag{29}$$

on the second reduced phase space $P_{n,m}$, where

$$\Delta\mathcal{E}^{(1)}(\nu, \pi_1) = \tfrac{1}{2}(\omega_- + \omega_+)\mu + \tfrac{1}{2}(\omega_- - \omega_+)\nu, \tag{30}$$

while $\Delta\mathcal{E}^{(2)}(\nu, \pi_1)$ is given in table 5. Furthermore, it is convenient to remove constant terms from $\Delta\mathcal{E}$, i.e., terms in (30) and table 5 and that depend only on $\mu = m, n$ and not on (ν, π_1). The resulting Hamiltonian function is

$$\mathcal{H}(\nu, \pi_1) = \Delta\mathcal{E}(\nu, \pi_1) - \Delta\mathcal{E}(0, 0), \tag{31}$$

which using (25) can be expressed also as a function of $(\mathbf{x}, \mathbf{y})$ on $\mathbb{S}^2 \times \mathbb{S}^2$. Note also that the dynamics on $P_{n,m}$ can be studied using $\mathcal{H}$ and the Poisson algebra of (ν, π_1, π_2).

4. Analysis of dynamical strata

In order to determine the type of fibres of the system for all (n, m, h) and obtain its $\mathcal{BD}$, it is sufficient to know the topology of the trajectories of the second reduced system on $P_{n,m}$ for different values h of $\mathcal{H}$. The idea of the analysis is as follows. Since we have a 1-DOF system, trajectories are level sets of $\mathcal{H}$ on $P_{n,m}$. To find them on $P_{n,m}$, we should simply find intersections

$$\lambda_{n,m,h} = \{\mathcal{H}(\nu, \pi_1) = h\} \cap P_{n,m} \tag{32}$$

of the constant h-level set of $\mathcal{H}$ and the reduced phase space $P_{n,m}$ in $\mathbb{R}^3$ with coordinate functions (ν, π_1, π_2). Due to the above-mentioned symmetry $\mathcal{T}_s$, it is sufficient to study projections of $\lambda_{n,m,h}$ on the $\mathbb{R}^2$ plane (ν, π_1), see figure 9. For each intersection $\lambda_{n,m,h}$ we find its preimage under $\mathcal{EM}$ in $\mathbb{R}^6$.

In the trivial case $m = \pm n$ both the space $P_{n,\pm n}$ and the intersection $\lambda_{n,\pm n,h}$ are the point $\nu = \pi_1 = \pi_2 = 0$. The critical energy is given by the value $\mathcal{H}(0, 0; m = \pm n) = 0$ of $\mathcal{H}$ at this point. In $\mathbb{R}^6$ the critical fibre is a Kepler ellipse.

For $0 \leqslant |m| < n$ the reduced space $P_{n,m}$ is typically a sphere, so the connected components of $\lambda_{n,m,h}$ are typically circles, and exceptionally, points or circles joined at a point (a figure-8). The points lift to relative equilibria $\mathbb{T}^2$, smooth circles lift to regular Lagrangian tori $\mathbb{T}^3$, while figure-8's lift to $\mathbb{T}^2_{\text{bi}} \times \mathbb{S}^1$, where the *bitorus* $\mathbb{T}^2_{\text{bi}}$ is depicted in figure 7 (right).

The case $m = 0$ is similar except for the fact that there are intersections $\lambda_{n,0,h_*}$ that contain one or both singular points $(\nu, \pi_1) = (\pm n, 0)$ of $P_{n,0}$. If $\lambda_{n,0,h_*}$ is a single singular point then it lifts to a *stable* Kepler ellipse in $\mathbb{R}^6$. If the intersection $\lambda_{n,0,h}$ is a circle that contains exactly one singular point of $P_{n,0}$ then it lifts in $\mathbb{S}^2 \times \mathbb{S}^2$ to a singly pinched torus $\mathbb{T}^2_{[1]}$, see figure 7 (left), and in $\mathbb{R}^6$ to $\mathbb{T}^2_{[1]} \times \mathbb{S}^1$. The singular point of $P_{n,0}$ that belongs to such $\lambda_{n,0,h}$ lifts in $\mathbb{R}^6$ to an *unstable* Kepler ellipse. Finally, if the intersection contains both singular points of $P_{n,0}$ then it lifts in $\mathbb{S}^2 \times \mathbb{S}^2$ to a doubly pinched torus $\mathbb{T}^2_{[2]}$, see figure 7 (centre), and in $\mathbb{R}^6$ to $\mathbb{T}^2_{[2]} \times \mathbb{S}^1$. The two singular points of $P_{n,0}$ in this case lift to two *unstable* Kepler ellipses. This completes the description of the most important intersections $\lambda_{n,m,h}$ that appear in the system and the corresponding fibres in $\mathbb{R}^6$.

We now are in a position to compute the $\mathcal{BD}$ of the system and obtain results announced in table 3 of section 2. To this end, we study the sets of regular and various critical energy–momentum values within the image of the $\mathcal{EM}$ map, and we construct the *bifurcation diagram* $\mathcal{BD}$. The sets of critical $\mathcal{EM}$ values are obtained by finding critical energies $h_c(n, m)$ for all possible $m \in [m', m''] \subseteq [-n, n]$. Typically $[m', m'']$ is a closed interval and the map $[m', m''] \to \mathbb{R}^2 : m \mapsto (m, h_c(n, m))$ defines smooth curve segments in the range of the $\mathcal{EM}$ map with fixed n. Once for given ns, f and g, all critical sets are found, we obtain the $\mathcal{BD}$ of the system.

As a straightforward application of the above discussion we consider systems of type A_2 and $A_{1,1}$. A_2 systems have been completely described in [4]. The intersections of constant energy levels with $P_{n,0}$ are given in figure 10 (left). One intersection contains both singular points of $P_{n,0}$ and lifts to $\mathbb{T}^2_{[2]} \times \mathbb{S}^1$. There are also two single-point intersections that correspond to the minimum and maximum energy and that lift to $\mathbb{T}^2$. These are all critical intersections. All other intersections $\lambda_{n,0,h}$ are smooth circles which correspond to regular values of $\mathcal{EM}$ and lift to $\mathbb{T}^3$. For all $m \neq \pm n$ there are also two critical intersections that correspond to the minimum and maximum energy just as in the case $m = 0$, while all other intersections are regular. Finally, for $m = \pm n$ there is only one critical single-point intersection. Putting together these facts we obtain the $\mathcal{BD}$ for A_2 systems in table 3.

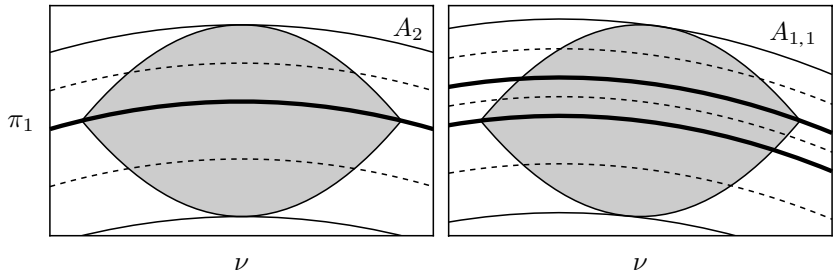

Figure 10. Different types of intersections $\lambda_{n,0,h}$ of the constant h-level sets of $\mathcal{H}$ of systems A_2 and $A_{1,1}$ with the reduced space $P_{n,0}$ projected on $\{\pi_2 = 0\}$. Dashed lines represent regular levels whose intersections with $P_{n,0}$ are smooth circles; thick black lines represent levels that go through the singular points $(\nu, \pi_1) = (\pm n, 0)$; critical levels that are tangent to $P_{n,0}$ are shown by thin solid curves. In the original space $\mathbb{R}^6$ regular intersections correspond to smooth $\mathbb{T}^3$, intersections containing singular points become pinched tori $\mathbb{T}^2_{[1]} \times \mathbb{S}^1$ (or $\mathbb{T}^2_{[2]} \times \mathbb{S}^1$ for type A_2), while tangency points lift to relative equilibria $\mathbb{T}^2$.

Breaking the specific $\mathbb{Z}_2$ symmetry of A_2 systems leads to $A_{1,1}$ systems. Intersections with $P_{n,0}$ for $A_{1,1}$ systems are depicted in figure 10, right. The most significant change is that there are now two critical intersections each one of which contains exactly one singular point of $P_{n,0}$. Each such intersection lifts to $\mathbb{T}^2_{[1]} \times \mathbb{S}^1$. All other critical intersections remain the same thus we obtain the $\mathcal{BD}$ for $A_{1,1}$ systems in table 3.

5. Applications in the quantum system

The classical Hamiltonian monodromy described in section 2.3 manifests itself in the corresponding quantum spectrum as explained in section 1.4. We quantize by replacing the classical Poisson algebra of $(\mathbf{x}, \mathbf{y})$ in (20) by its quantum counterpart and all classical quantities by the corresponding quantum operators marked by hats, e.g., $\hat{\mu}$. If quantum operators do not commute, such replacement becomes ambiguous. When this happens, we symmetrize the corresponding terms, e.g., $ab \to \frac{1}{2}(\hat{a}\hat{b} + \hat{b}\hat{a})$. Subsequently, we compute the joint quantum spectrum of the commuting operators $\widehat{\Delta\mathcal{E}}$ and $\hat{\mu}$ from the second normalized system. Further we compute the spectrum of the first normal form $\widehat{\Delta E}$. In order to compare this spectrum with the joint spectrum of $\widehat{\Delta\mathcal{E}}$ and $\hat{\mu}$ we should have the analogue of $\hat{\mu}$ in the first normalized system so that we can label the eigenstates. This analogue can be obtained by inverting at the classical level the normal form transformation and computing the preimage μ' of μ as a formal power series in $(\mathbf{x}, \mathbf{y})$. However since $\widehat{\Delta E}$ and $\hat{\mu}'$ do *not* commute we can only obtain an approximate joint spectrum using the expectation values $\langle\hat{\mu}'\rangle$ of $\hat{\mu}'$ on the eigenstates of $\widehat{\Delta E}$. We compare the resulting joint spectra $(\widehat{\Delta\mathcal{E}}, \hat{\mu})$, $(\widehat{\Delta E}, \langle\hat{\mu}'\rangle)$.

A number of comments may be due here with regard to our quantum study. We compute quantum spectra from the classical normal form. Classical and quantum normalizations can be formulated in a similar way. The direct analogue of the classical Lie series transformation [52, 54] is the Van Vleck method [55] which is, essentially, the Lie transform method with Poisson brackets replaced by quantum commutators. However, the latter lead (typically, cf G. C. Wick's theorem) to nonhomogeneous terms of order $(\hbar ns)^k$ with $\hbar = 1$ au that include (q, p) monomials of degrees less or equal $k + 2$ and which agree with the classical expression only to the principal degree $k + 2$. In other words, comparing to the 'exact' quantum normalization we may expect small $O(\hbar ns)$ corrections in each order. Nevertheless, because we only study

structurally stable systems and keep $\hbar ns$ sufficiently small, we argue that these corrections are inessential.

Our comparison of quantum spectra to the classical bifurcation diagram relies on the EBK principle. It is common knowledge that for any such comparison to be meaningful, and for the typical structures in the classical phase space and in the bifurcation diagram $\mathcal{BD}$ to be visible in the quantum spectra, $\hbar$ has to be small compared to the structures in questions. In our case this is achieved by choosing $n \gg \hbar = 1$ compensated by a sufficiently small value of s. The quantum–classical agreement in our figures shows clearly enough how well these choices work. The discrepancies between the EBK and the exact quantum results are limited to small neighbourhoods of singular $\mathcal{EM}$ values invisible in the scale of our figures. Such discrepancies may, perhaps, be of more interest for structurally unstable systems, but, again, we avoid those here. A study of such fine details is far beyond the scope of the paper. For the contemporary quantitative results which may provide further guidance on what low values of n can be taken see [56], and references therein. One should note that presently, these results concern exclusively energies and have yet to be extended to the expectation values of approximate integrals (such as momentum μ in our case) introduced by normalization.

The question that we worry more about and that we address in more detail is whether our values of ns are low enough for our normal forms to be trustworthy and for the EBK principle to be relied upon. Specifically, for certain particular choices we check numerically using eigenfunctions of the complete system that the dispersion of the expectation values $\langle\hat{\mu}\rangle$ is considerably smaller than $\hbar$. We will also assume that the broadening of energy levels that occurs in the presence of the electric field due to tunnelling can be neglected, i.e., the 'width' of the level is much smaller than $\hbar$.

Further brief comments may perhaps be appropriate here as to the properties of the quantum states with given values of energy and $\langle\hat{\mu}\rangle$. If the momentum μ is a well-conserved quantity, its value $\langle\hat{\mu}\rangle$ should characterize such properties of the eigenstate as the probabilities of specific spectroscopic transitions or collision propensity rules. The dispersion of $\langle\hat{\mu}\rangle$ would give indication of how well these specific properties are pronounced. Further properties due to localization depend on the position of the node of the joint spectrum lattice representing the eigenstate in question with respect to the critical value set(s) of the classical $\mathcal{BD}$. Nodes close to the $\mathcal{BD}$ boundaries represent oscillatory states strongly localized at relative equilibria $\mathbb{T}^2$ or, Keplerian relative equilibria $\mathbb{S}^1$ (in $\mathbb{R}^6$). For B_0 (near the quadratic Zeeman effect) and B_1-type systems we should expect properties typically found in situations with symmetric and asymmetric double wells respectively. For quantum states represented by nodes close to the bitorus critical lines we should observe strong tunnelling effects and delocalization. Due to chaos destroying the respective hyperbolic relative equilibria and the irregular dynamics in their immediate neighbourhoods, we should expect further disagreement with the torus quantization data. Finally, quantum wavepackets with energy–momentum maxima near the unstable focus–focus equilibria (such as in the A_1 and $A_{1,1}$ types) represent states with nontrivial long-time behaviour [57].

5.1. Quantum lattices

Figure 12 shows the joint energy–momentum spectra for different parameter values which correspond to different qualitative types A_1, $A_{1,1}$, A_2, B_1 and B_0 of systems in the 1:1 zone described in section 2. First of all we like to note that the joint spectrum for the case of the exact 1:1 resonance (strictly orthogonal fields), i.e., for systems of type A_2 and B_0, was already computed in [4] for energy-scaled fields and for the second normalized Kustaanheimo–Stiefel Hamiltonian. Comparing to figure 9 of [4], we can see that these spectra are qualitatively

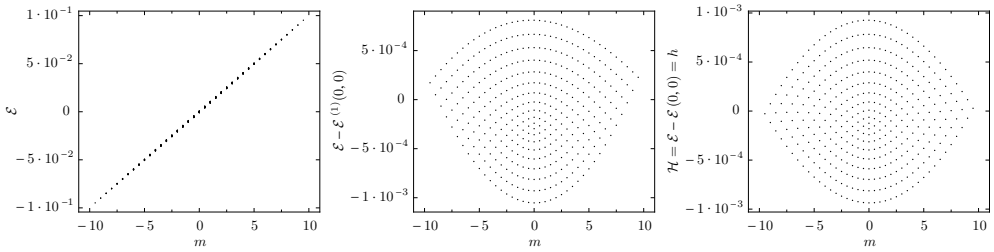

Figure 11. The joint spectrum for a type A_2 system. Parameters are $s = 10^{-2}$, $j = 19/2, \hbar = 1/2, d = 0$ and $a^2 = 0.4$ (same as the type A_2 system in figure 12). Left panel: no dynamically constant (i.e., dependent only on m and n) terms have been subtracted from the energy correction $\Delta\mathcal{E}$. Centre panel: only the first-order dynamically constant term $\Delta\mathcal{E}^{(1)}(0,0)$ has been subtracted. Right panel: $\mathcal{H}$ is plotted, i.e., the complete dynamically constant term $\Delta\mathcal{E}(0,0)$ has been subtracted, cf table 5 and equations (29)–(31).

identical to those computed here. The reason is that, in the exact 1:1 resonance, the difference between the energy correction $\Delta\mathcal{E}$ we use here and the second normal form used in [4] is a function of (m, n). At the same time, exact correspondence for the values of the unscaled fields in the two calculations is difficult to establish because the energy slightly varies while n is fixed.

For the sake of comparison to real quantum energies of the perturbed hydrogen atom which one may obtain for example by solving the Schrödinger equation directly for the Hamiltonian in (1), we like also to remind that the energies here are computed *without* the dynamically constant (i.e., dependent only on m and n) terms $\Delta\mathcal{E}(0,0)$ of $\Delta\mathcal{E}$, see section 3.3, table 5. In order to illustrate the effect on the spectrum of the subtraction of such dynamically constant terms from $\Delta\mathcal{E}$ we depict in figure 11 the joint spectrum for an A_2 system subtracting different such constant terms. In the left panel $\Delta\mathcal{E}$ is plotted without subtracting any terms and the joint spectrum appears as almost a line (linear Stark–Zeeman structure). The slope of the latter can be estimated from the values of $\Delta\mathcal{E}^{(1)}$ at relative equilibria for $m = \pm n$, $(\nu, \pi_1) = (0, 0)$, given by

$$\Delta\mathcal{E}^{(1)}(0,0) = \tfrac{1}{2}m(\omega_- + \omega_+).$$

The total energy span $n(\omega_- + \omega_+)$ for one n-shell is determined by the above term and is much larger than the second-order splitting barely visible as the 'width' of the line. In the middle panel of figure 11, the above linear-in-m term is subtracted, and in the bottom panel, the energy correction $\mathcal{H}$, see (31), is plotted by subtracting all dynamically constant terms from $\Delta\mathcal{E}$. We use the latter representation in all our other figures of $\mathcal{BD}$ and joint spectra.

In type A_0 systems, the joint spectrum is a regular $\mathbb{Z}^2$ lattice, see figure 12. This confirms the classical result in section 2.3. We have two globally defined quantum numbers. In the B_0 systems (either B_0' or B_0'') the base space consists of two disjoint regions marked in figure 12 by light and dark grey shade. The lattice within each region is regular. In all the other cases: A_1, $A_{1,1}$, A_2 and B_1, the joint spectrum is not a regular lattice and these systems have monodromy. We discuss monodromy further in section 5.3.

5.2. Comparison of spectra for the first and second normalized systems

Further interesting information can be conveyed by the comparison of the joint spectrum lattices of $(\widehat{\Delta\mathcal{E}}, \hat{\mu})$ (figure 12, left column) to that computed for $\widehat{\Delta E}$ and $\langle\hat{\mu}'\rangle$ (figure 12,

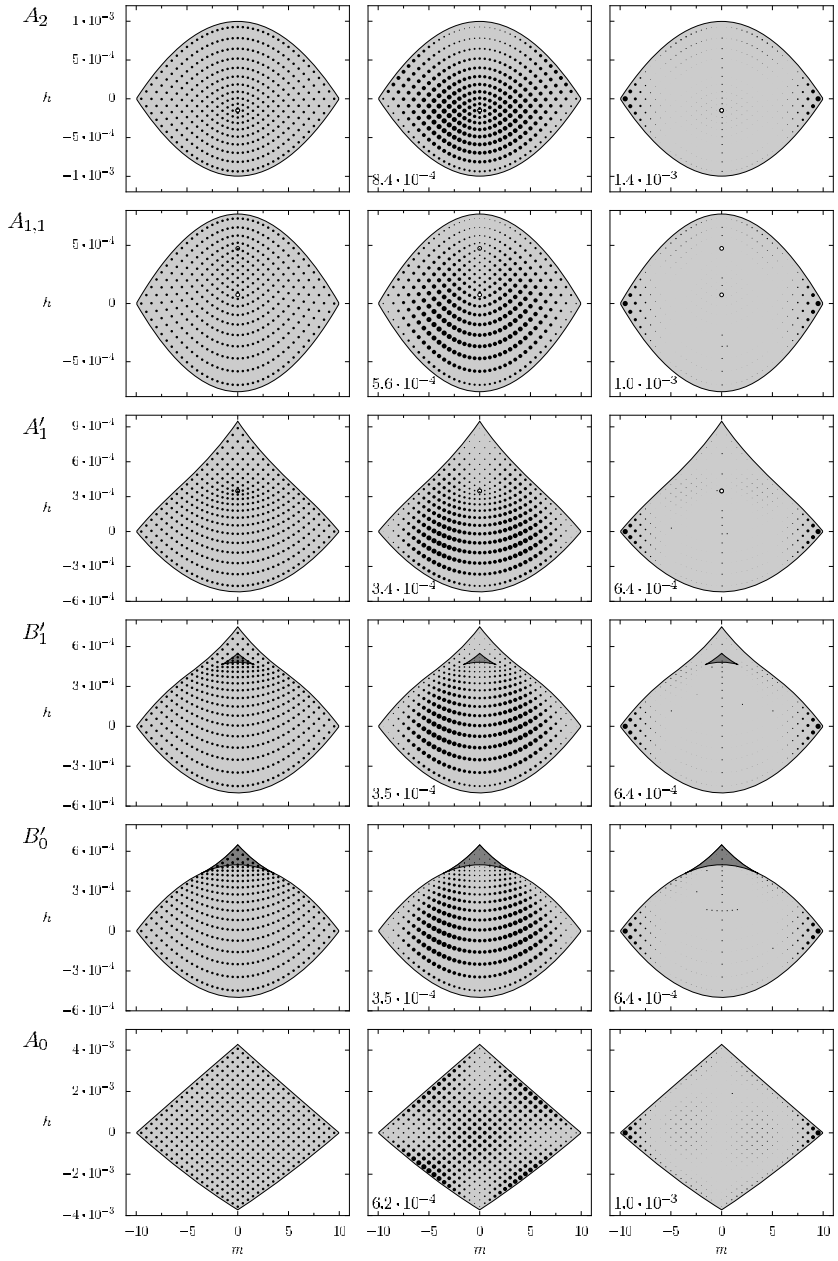

Figure 12. Joint spectrum for the second and first normal forms. In all cases $s = 10^{-2}$, $j = 19/2$ and $\hbar = 1/2$ so that $n = 2\sqrt{j(j+1)}\hbar \simeq 10$. $\mathcal{BD}$ types and the corresponding parameter values are: type $A_2, d = 0, a^2 = 0.4$ (figure 11), type $A_{1,1}, d = 0.002, a^2 = 0.3$, type $A_1', d = 0.003, a^2 = 0.2$, type $B_1', d = 0.001, a^2 = 0.2$, type $B_0', d = 0, a^2 = 0.2$ and type $A_0, d = 0.04, a^2 = 0.3$. In each row the first panel represents the joint spectrum for the second normal form. The second panel represents the spectrum for the first normal form where the size of the lattice points represents the uncertainty $\Delta\hat{\mu}'$ for each eigenstate. In the third panel we plot the difference $\langle\hat{\mu}'\rangle$ from the closest value of $m_q\hbar$ for half integer m_q. The number that appears at the lower left corner of the second and third panels is the maximum value of the plotted quantity $\Delta\hat{\mu}'$ and $|\langle\hat{\mu}'\rangle - m_q\hbar|$ respectively.

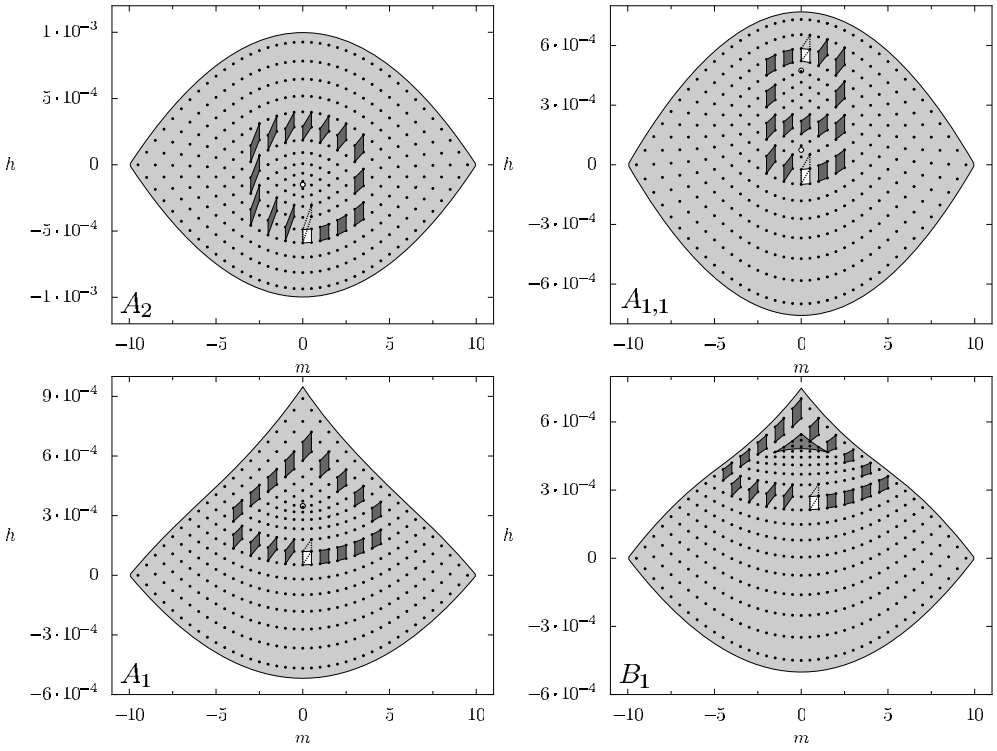

Figure 13. Elementary cell diagrams for types of systems with monodromy. In each case the initial elementary cell is represented by a white filled cell. This initial cell is parallel transported in a counterclockwise direction around a critical value or a set of critical values of the $\mathcal{EM}$ map. The final cell is represented by a cell with dotted border.

second column). In the latter figure, each eigenstate is represented as a filled disc with the radius given by uncertainty

$$\Delta\hat{\mu}' = \sqrt{\langle(\hat{\mu}')^2\rangle - \langle\hat{\mu}'\rangle^2}. \tag{33}$$

For the perturbation magnitude s which we used, both the uncertainties and discrepancies $|m_q\hbar - \langle\hat{\mu}'\rangle|$ (see figure 12 last column) are very small—they would have been invisible in the scale of the figure without artificial magnification. Here m_q is the half-integer that minimizes $|m_q\hbar - \langle\hat{\mu}'\rangle|$; it is essentially the nearest eigenvalue of $\hat{\mu}'$. This close agreement indicates that at such s, the second normalization procedure is perfectly valid and that the intra-shell chaotic dynamics can be safely neglected for our purposes.

We can also see that the uncertainties are small compared to 1 and therefore the approximate joint spectrum is well defined. Furthermore normalization works visibly better near the elliptic Keplerian equilibria with $m = \pm n$.

5.3. Quantum monodromy

To uncover monodromy of systems A_2, $A_{1,1}$, A_1 and B_1, see figure 13, we parallel transport an elementary cell around a closed path encircling the corresponding critical value of the energy–momentum map (cf section 1.4). The path goes counterclockwise within the locally regular domain of the lattice, so that at each small step the transport of the cell is unambiguously

defined. After closing the path, the final elementary cell is compared to the initial one. In all depicted cases, initial and final cells differ thus proving nontrivial monodromy.

Specifically an elementary cell can be defined by two elementary vectors u_1 and u_2, giving the increment of each local quantum number by 1. The transformation between the initial (u_1, u_2) and the final (u_1', u_2') is given by a 2×2 matrix in $\mathrm{GL}(2, \mathbb{Z})$ which is the inverse transpose of the monodromy matrix M, see [21, 41, 58]. The same approach can be generalized to three-dimensional lattices. In that way, we can confirm the results of the classical analysis in section 2.3 for M in (9) and (10). Note that up to the natural increase in the number of nodes near the boundaries, quantum lattices for all systems extend trivially in the third dimension n. This is in agreement with the classical result $k_N = 0$ in section 2.3. So here we only discuss two-dimensional sublattices.

In all cases in figure 13 we choose the initial cell so that the vector u_1 is vertical, i.e., along axis h, and u_2 is nearly horizontal. The vector u_1 does not change while u_2 changes so that $u_2' = u_2 + k u_1$ where k is the same as in (10).

In the A_2 system we observe that $k = 2$, as was first seen in [4]. In the $A_{1,1}$ system we consider just as in the classical case two different paths Γ^- and Γ^+ around the critical values o^- and o^+ respectively, see section 2.3. For each path we find that $k = 1$. From the same picture we can deduce that the monodromy matrix for the path $\Gamma = \Gamma^- + \Gamma^+$ that goes around both o^- and o^+ has $k = 2$.

In the cases A_1 and B_1 (see figure 13, where only the particular cases A_1' and B_1' are depicted) the value of k for a path that goes around the isolated critical value or the segment $\mathcal{C}$ of critical values respectively is again 1. In the case B_1 the joint spectrum can be decomposed into two parts that correspond to the two leaves of the unfolded $\mathcal{BD}$ in figure 2 (right). The lattice corresponding to the 'smaller' leaf is regular. Monodromy is only related to the lattice corresponding to the bigger 'lower' leaf. Note that the A_1 system has monodromy of the most standard kind, cf figure 4, while the B_1 monodromy has been observed before in floppy molecules [59], deformed spherical pendulum [24] and others [32, 60]. The existence of the $A_{1,1}$ case has been understood by [61].

6. Discussion and perspectives

A reader, who is familiar with the rich history of our subject, may suggest that its perturbation theory analysis was completed in the 10 years after the second normalized Hamiltonian ($\Delta\mathcal{E}$ in our notation) was obtained in [62–67], that this theory is quite simple and reliable, and that nothing 'new' can be expected in this direction, especially since we work here with the same second order of the perturbation theory. However, a more careful look back at the past work shows that nothing can be more illusory. In this system with three degrees of freedom and three parameters, the difficulty of *global* analysis—in terms of both the phase-space and the parameter-space structures, is quite substantial. Indeed, very simple, almost basic global aspects of this parametric family of fundamental atomic systems, such as resonances of the linearized system, monodromy, and more generally—structurally stable types of possible toric fibrations and corresponding joint quantum spectra, become understood only now—80 years after Pauli [1] and 25 years after Solov'ev [62, 63, 65–67] and Herrick [64].

In this paper and in the recent [28], the description, classification and characterization of different near-orthogonal perturbations of the hydrogen atom started in [26, 27] is completed. It is summarized in section 2 and illustrated in section 5. This classification relies on the second-order $\Delta\mathcal{E}$. Finer details may appear at higher orders where the three-dimensional dynamical strata (whose constant-$n\mathcal{BD}$ sections are given in table 3) and the nontrivial symmetry strata of

the parameter space will not change qualitatively, but some of their boundaries may transform into small regions with more complex $\mathcal{BD}$.

An idea of what may happen can be obtained from [25] where the complete analysis of the transition between A_2 and B_0 required normalizing to order 4. Other bifurcations in the 1:1 zone should be studied in the similar way. Particularly complex can be the analysis of the near-Stark region and the region near the intersections of the boundaries of several dynamical strata (see figure 5).

The other remaining important question is the 'size' or 'width' of the 1:1 zone, which is given by $d_{\max}$. With growing ns, the dynamical size of the zone, i.e., the interval of d in which we can treat the system as a detuned 1:1 resonance, shrinks. This dependence for the 1:1 and other zones is subject of ongoing studies.

The role of non-integrability should be further uncovered and we should be able to define a limiting maximum value of (ns) up to which the approach based on integrable approximation is meaningful. Thus for example, within our integrable approximation, the parallel stratum near the Zeeman limit is indistinguishable dynamically from the neighbouring B_1' and A_1''. However, due to their exact axial Lie symmetry, parallel field systems should eventually differ in certain ways from other non-integrable systems with three degrees of freedom. In particular, outside the 1:1 zone, systems in the $\parallel$ symmetry stratum become superintegrable after second normalization and have global action–angle coordinates. So, systems in the $\parallel$ stratum are indistinguishable only within the 1:1 zone because there the 1:1 symmetry and the axial symmetry act in the same way.

Finally, the most important direction of future research is the global study of other resonance zones that correspond to different mutual orientations of the fields. Particularly interesting is the 1:2 zone [68]. Preliminary analysis [26] has pointed to the existence of fractional monodromy [41, 43–45] for systems in the 1:2 zone.

Acknowledgments

The authors would like to thank B I Zhilinskií and H W Broer for useful discussions. KE acknowledges support from the NWO mathematics cluster NDNS$^+$.

References

[1] Pauli W 1926 Über das Wasserstoffspektrum vom Standpunkt der neuen Quantenmechanik *Z. Phys.* A **36** 336–63
[2] Solov'ev E A 1983 Second-order perturbation theory for the hydrogen atom in crossed electric and magnetic fields *Zh. Eksp. Teor. Fiz.* **85** 109
[3] Herrick D R 1982 Symmetry of the quadratic Zeeman effect for hydrogen *Phys. Rev.* A **26** 323–9
[4] Cushman R H and Sadovskií D A 2000 Monodromy in the hydrogen atom in crossed fields *Physica* D **142** 166–96
[5] Gourlay M J, Uzer T and Farrelly D 1993 Asymmetric-top description of Rydberg electron dynamics in crossed external fields *Phys. Rev.* A **47** 3113–7
[6] Flöthmann E, Main J and Welge K H 1994 The Kepler ellipses of the hydrogen atom in crossed electric and magnetic fields *J. Phys. B: At. Mol. Opt. Phys.* **27** 2821–33
[7] von Milczewski J and Uzer T 1997 Canonical perturbation treatment of a Rydberg electron in combined electric and magnetic fields *Phys. Rev.* A **56** 220–31
[8] Main J, Schwacke M and Wunner G 1998 Hydrogen atom in combined electric and magnetic fields with arbitrary mutual orientations *Phys. Rev.* A **57** 1149–57
[9] Berglund N and Uzer T 2001 The averaged dynamics of the hydrogen atom in crossed electric and magnetic fields as a perturbed Kepler problem *Found. Phys.* **31** 283–326
[10] Uzer T 2001 Rydberg electrons in crossed fields: A paradigm for nonlinear dynamics beyond two degrees of freedom *Phys. Scr.* **90** 176–84

[11] Wiebusch G, Main J, Krüger K, Rottke H, Holle A and Welge K H 1989 Hydrogen atom in crossed magnetic and electric fields *Phys. Rev. Lett.* **62** 2821–4
[12] von Milczewski J, Diercksen G H F and Uzer T 1996 Computation of the Arnol'd web for the hydrogen atom in crossed electric and magnetic fields *Phys. Rev. Lett.* **76** 2890–3
[13] von Milczewski J and Uzer T 1997 Chaos and order in crossed fields *Phys. Rev.* E **55** 6540–51
[14] Rakovic M J, Uzer T and Farrelly D 1998 Classical and quantum mechanics of an integrable limit of the hydrogen atom in combined circularly polarized microwave and magnetic fields *Phys. Rev.* A **57** 2814–31
[15] Bartsch T, Main J and Wunner G 2003 Closed orbits and their bifurcations in the crossed-field hydrogen atom *Phys. Rev.* A 67
[16] Bartsch T, Gekle S, Main J and Uzer T 2007 Gluing torus families across a singularity: the lens space for the hydrogen atom in crossed fields *Prog. Theor. Phys. Suppl.* **166** 45–55
[17] Gekle S, Main J, Bartsch T and Uzer T 2007 Hydrogen atom in crossed electric and magnetic fields: phase space topology and torus quantization via periodic orbits *Phys. Rev.* A **75** 23406-1–13
[18] Rink B W 2004 A Cantor set of tori with monodromy near a focus–focus singularity *Nonlinearity* **17** 347–56
[19] Broer H, Cushman R, Fassò F and Takens F 2007 Geometry of KAM tori for nearly integrable Hamiltonian systems *Ergodic Theory Dyn. Syst.* **27** 725–41
[20] Duistermaat J J 1980 On global action–angle coordinates *Commun. Pure Appl. Math.* **33** 687–706
[21] Vũ Ngọc S 1999 Quantum monodromy in integrable systems *Commun. Math. Phys.* **203** 465–79
[22] Cushman R H and Duistermaat J J 2001 Non-Hamiltonian monodromy *J. Diff. Eqns* **172** 42–58
[23] Zung N T 1997 A note on focus–focus singularities *Diff. Geom. Appl.* **7** 123–30
[24] Efstathiou K 2005 *Metamorphoses of Hamiltonian Systems with Symmetries (Lecture Notes in Mathematics* vol 1864*)* (Berlin: Springer)
[25] Efstathiou K, Cushman R H and Sadovskiĭ D A 2004 Hamiltonian Hopf bifurcation of the hydrogen atom in crossed fields *Physica* D **194** 250–74
[26] Efstathiou K, Sadovskiĭ D A and Zhilinskiĭ B I 2007 Classification of perturbations of the hydrogen atom by small static electric and magnetic fields *Proc. R. Soc. Lond.* A **463** 1771–90
[27] Schleif C R and Delos J B 2007 Monodromy and the structure of the energy spectrum of hydrogen in near perpendicular electric and magnetic fields *Phys. Rev.* A **76** 013404
[28] Schleif C R and Delos J B 2008 Semiclassical theory of the structure of the hydrogen spectrum in near-perpendicular electric and magnetic fields: derivations and formulas for Einstein–Brillouin–Keller–Maslov quantization and description of monodromy *Phys. Rev.* A **77** 043422–28
[29] Karasev M and Novikova E 2005 Algebras with polynomial commutation relations for the Zeeman–Stark effect in the hydrogen atom *Theor. Math. Phys.* **142** 447–69
[30] Sadovskiĭ D A and Zhilinskiĭ B I 1999 Monodromy, diabolic points, and angular momentum coupling *Phys. Lett.* A **256** 235–44
[31] Hansen M S, Faure F and Zhilinskiĭ B I 2007 Fractional monodromy in systems with coupled angular momenta *J. Phys. A: Math. Theor.* **40** 13075
[32] Davison C M, Dullin H R and Bolsinov A V 2007 Geodesics on the ellipsoid and monodromy *J. Geom. Phys.* **57** 2437–54
[33] Sadovskiĭ D A and Zhilinskiĭ B I 1998 Tuning the hydrogen atom in crossed fields between the Zeeman and Stark limits *Phys. Rev.* A **57** 2867–84
[34] Efstathiou K, Lukina O V and Sadovskiĭ D A 2009 Normalization and global analysis of perturbations of the hydrogen atom by weak electric and magnetic fields (in preparation)
[35] Gaeta G 2001 Algorithmic reduction of Poincaré–Dulac normal forms and Lie algebraic structure *Lett. Math. Phys.* **57** 41–60
[36] Gaeta G 1999 Poincaré renormalized forms *Ann. Inst. H. Poincaré* **70** 461–514
[37] Gaeta G 1997 Reduction of Poincaré normal forms *Lett. Math. Phys.* **42** 103–14
[38] Goldstein H 1980 *Classical Mechanics* 2nd edn (Reading, MA: Addison-Wesley)
[39] Bolsinov A V and Fomenko A T 2004 *Integrable Hamiltonian Systems: Geometry, Topology, Classification* (Boca Raton, Fl: Chapman and Hall/CRC)
[40] Abraham R and Marsden J 1978 *Foundations of Mechanics* 2nd edn (Reading, MA: Addison-Wesley)
[41] Nekhoroshev N N, Sadovskiĭ D A and Zhilinskiĭ B I 2006 Fractional Hamiltonian monodromy *Ann. H. Poincaré* **7** 1099–211
[42] Zhilinskiĭ B I 2005 Interpretation of quantum Hamiltonian monodromy in terms of lattice defects *Acta Appl. Math.* **87** 281–307
[43] Nekhoroshev N N, Sadovskiĭ D A and Zhilinskiĭ B I 2002 Fractional monodromy of resonant classical and quantum oscillators *C. R. Acad. Sci. Paris, Ser.* I **335** 985–8
[44] Efstathiou K, Cushman R H and Sadovskiĭ D A 2007 Fractional monodromy in the 1: − 2 resonance *Adv. Math.* **209** 241–73

[45] Sugny D, Mardešić P, Pelletier M, Jebrane A and Jauslin H R 2008 Fractional Hamiltonian monodromy from a Gauss–Manin monodromy *J. Math. Phys.* **49** 042701–35
[46] Sadovskiĭ D A and Zhilinskiĭ B I 2007 Hamiltonian systems with detuned 1:1:2 resonance: manifestation of bidromy *Ann. Phys.* **322** 164–200
[47] Michel L and Zhilinskiĭ B I 2001 Rydberg states of atoms and molecules. Basic group-theoretical and topological analysis *Phys. Rep.* **341** 173–264
[48] Cushman R H and Bates L 1997 *Global Aspects of Classical Integrable Systems* (Basle: Birkhäuser)
[49] Cushman R H and San V N 2002 Sign of the monodromy for Liouville integrable systems *Ann. H. Poincaré* **3** 883–94
[50] van der Meer J C 1985 *The Hamiltonian Hopf Bifurcation (Lecture Notes in Mathematics* vol 1160*)* (New York: Springer)
[51] Robnik M and Schrüfer E 1985 Hydrogen atom in a strong magnetic field—calculation of the energy levels by quantizing the normal form of the regularized Kepler Hamiltonian *J. Phys. A: Math. Gen.* **18** L853–9
[52] Gröbner W 1960 *Die Lie-Reihen und ihre Anwendungen* (Berlin: Deutscher Verlag der Wissenschaftern)
[53] Meyer K R and Hall G R 1991 *Introduction to Hamiltonian Dynamical Systems and the N-Body Problem (Applied Mathematical Sciences* vol 90*)* (New York: Springer)
[54] Deprit A 1969 Canonical transformations depending on a small parameter *Cel. Mech.* **1** 12–30
[55] Shavitt I 1980 Quasi-degenerate perturbation theories—a canonical Van-Vleck formalism and its relationship to other approaches *J. Chem. Phys.* **73** 5711
[56] Charles L and Vũ Ngọc San 2008 Spectral asymptotics via the semiclassical Birkhoff normal form *Duke Math. J.* **143** 463–511
[57] Sanrey M, Joyeux M and Sadovskiĭ D A 2006 Classical and quantum-mechanical plane switching in CO_2 *J. Chem. Phys.* **124** 074318
[58] Efstathiou K, Joyeux M and Sadovskiĭ D A 2004 Global bending quantum number and the absence of monodromy in the HCN↔CNH molecule *Phys. Rev.* A **69** 032504
[59] Joyeux M, Sadovskiĭ D A and Tennyson J 2003 Monodromy of the LiNC/NCLi molecule *Chem. Phys. Lett.* **382** 439–42
[60] Waalkens H, Junge A and Dullin H R 2003 Quantum monodromy in the two-centre problem *J. Phys. A: Math. Gen.* **36** L307–14
[61] Schleif C R and Delos J B 2006 Private communication
[62] Solov'ev E A 1981 Approximate integral of motion of H atoms in a magnetic field *Pis'ma ZhETF* **34** 278–81
[63] Solov'ev E A 1982 Hydrogen atom in a weak magnetic field *Zh. Eksp. Teor. Fiz.* **82** 1762–71
[64] Herrick D R 1982 Symmetry of the quadratic Zeeman effect for hydrogen *Phys. Rev.* A **26** 323–9
[65] Grozdanov T P and Solov'ev E A 1982 Semi-classical quantization of the hydrogen atom in crossed electric and magnetic fields *J. Phys. B: At. Mol. Phys.* **15** 1195–204
[66] Solov'ev E A 1983 Second-order perturbation theory for a hydrogen atom in crossed electric and magnetic fields *Zh. Eksp. Teor. Fiz.* **85** 109–14
[67] Solov'ev E A 1983 Second-order perturbation theory for a hydrogen atom in crossed electric and magnetic fields *Sov. Phys.—JETP* **58** 63–6
[68] Efstathiou K, Lukina O V and Sadovskiĭ D A 2008 Most typical 1:2 resonant perturbation of the hydrogen atom by weak electric and magnetic fields *Phys. Rev. Lett.* at press